

# Subduction-zone structure and magmatic processes beneath Costa Rica constrained by local earthquake tomography and petrological modelling

S. Husen,<sup>1,\*</sup> R. Quintero,<sup>2</sup> E. Kissling<sup>1</sup> and B. Hacker<sup>3</sup>

<sup>1</sup>Institute of Geophysics, ETH Hoenggerberg, Zurich, Switzerland

<sup>2</sup>Observatorio Vulcanológico de Costa Rica (OVSICORI-UNA), Costa Rica

<sup>3</sup>Department of Geological Science, University of California, Santa Barbara, USA

Accepted 2003 February 26. Received 2002 December 22; in original form 2002 May 24

## SUMMARY

A high-quality data set of 3790 earthquakes were simultaneously inverted for hypocentre locations and 3-D *P*-wave velocities in Costa Rica. Tests with synthetic data and resolution estimates derived from the resolution matrix indicate that the velocity model is well constrained in central Costa Rica to a depth of 70 km; northwestern and southeastern Costa Rica are less well resolved owing to a lack of seismic stations and seismicity. Maximum H<sub>2</sub>O content and seismic wave speeds of mid-ocean ridge basalt and harzburgite were calculated for metamorphic phase transformations relevant to subduction. Both the 3-D *P*-wave velocity structure and petrological modelling indicate the existence of low-velocity hydrous oceanic crust in the subducting Cocos Plate beneath central Costa Rica. Intermediate-depth seismicity correlates well with the predicted locations of hydrous metamorphic rocks, suggesting that dehydration plays a key role in generating intermediate-depth earthquakes beneath Costa Rica. Wadati–Benioff zone seismicity beneath central Costa Rica shows a remarkable decrease in maximum depth toward southeastern Costa Rica. The presence of asthenosphere beneath southeastern Costa Rica, which entered through a proposed slab window, may explain the shallowing of seismicity due to increased temperatures and associated shallowing of dehydration of the slab. Tomographic images further constrain the existence of deeply subducted seamounts beneath central Costa Rica. Large, low *P*-wave velocity areas within the lower crust are imaged beneath the southeasternmost volcanoes in central Costa Rica. These low velocities may represent anomalously hot material or even melt associated with active volcanism in central Costa Rica. Tomographic images and petrological modelling indicate the existence of a shallow, possibly hydrated mantle wedge beneath central Costa Rica.

**Key words:** crustal structure, earthquake location, mineralogy, seismic tomography, subduction.

## INTRODUCTION

Much progress has been made in recent years in resolving the physical and chemical processes of subduction zones. Improved data sets and methods have enabled 3-D imaging of subduction zones with great detail (Graeber & Asch 1999; Zhao *et al.* 2000; Haberland & Rietbrock 2001; Nakajima *et al.* 2001). High *P*-wave velocities and a low attenuation outline the subducting oceanic lithosphere to depths over 150 km. Low *P*-wave velocities, high *P*- to *S*-wave ratios and low attenuation are taken as an indication of partial melt and are imaged in the mantle wedge and in the crust beneath active vol-

canoes. Thermal and petrological modelling provides further constraints on the fact that intermediate-depth earthquakes are linked to metamorphic reactions and that subduction-zone magmatism is related to fluid release. As the oceanic lithosphere subducts it undergoes a series of metamorphic phase transformations that release H<sub>2</sub>O (Peacock 1996; Hacker *et al.* 2003a). The release of H<sub>2</sub>O may enable the generation of intermediate-depth earthquakes by dehydration (Kirby *et al.* 1996; Hacker *et al.* 2003b), which in turn may be important for the transport of fluid into the overlying mantle wedge (Davies 1999). The existence of hydrous fluid in the mantle wedge lowers the solidus of mantle peridotite, triggering partial melting and volcanism (Gill 1981).

Subduction of the Cocos Plate, tectonism along the Central Costa Rica Deformed Belt (Marshall *et al.* 2000), and active

\*Now at: Department of Geology and Geophysics, University of Utah, 135S 1460 East, Salt Lake City, UT 84122, USA. E-mail: shusen@mines.utah.edu

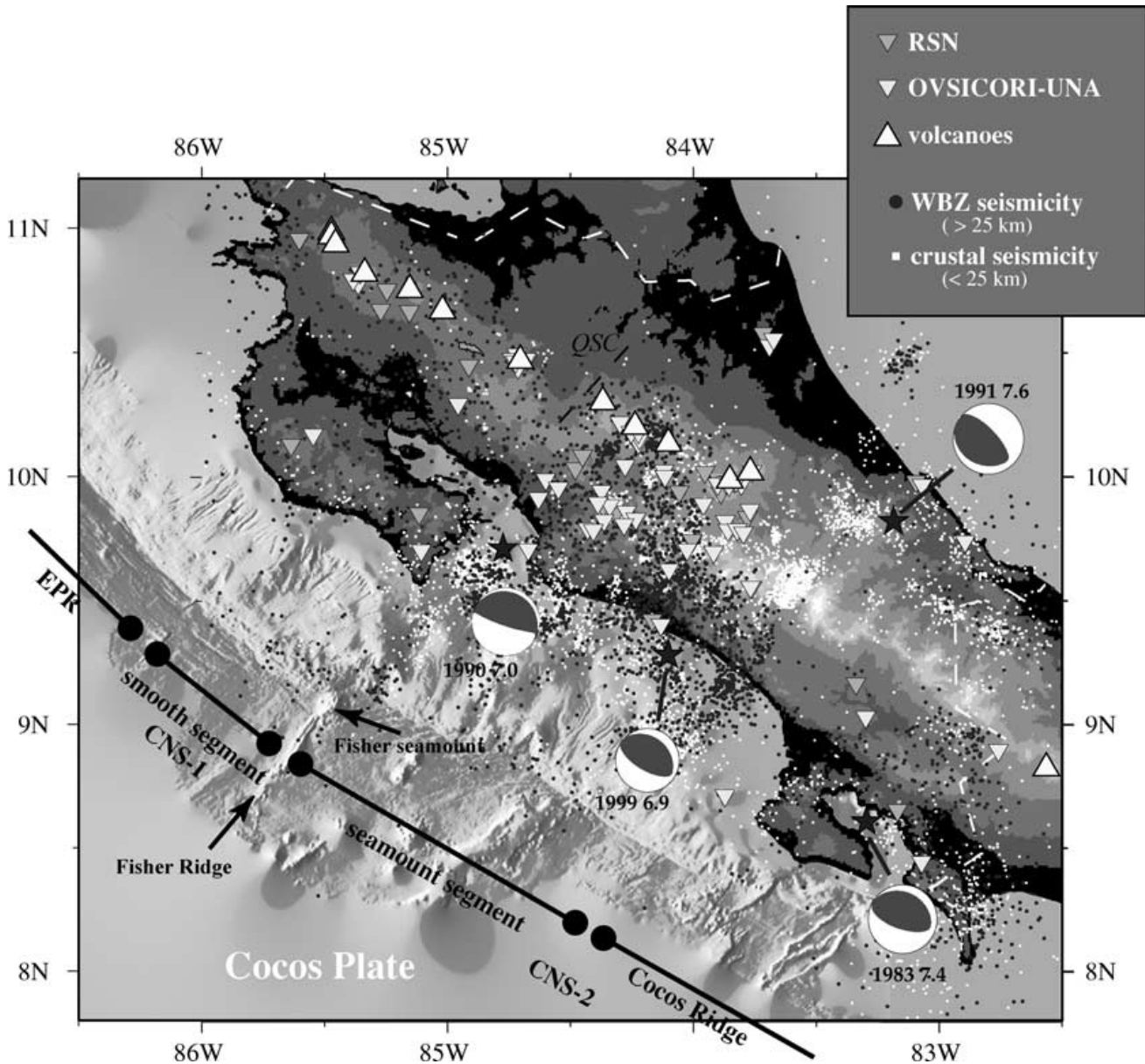


**Figure 1.** Seismicity and station distribution from 1984 to 1997 in Costa Rica. Seismicity was recorded by the OVSICORI-UNA network administered by the Universidad de Nacional and Red Sismológica Nacional (RSN). Fault-plane solutions of large events ( $M_w > 6.5$ ) are taken from Harvard CMT catalogue. Bathymetry is modified after von Huene *et al.* (2000). Main tectonic segments after von Huene *et al.* (2000) and origin of the oceanic crust after Barckhausen *et al.* (2001). EPR, East Pacific Rise; CNS-1 Cocos–Nazca Spreading Center 1; CNS-2 Cocos–Nazca Spreading Center 2. QSC Quesada Sharp Contortion.

volcanism cause a high seismicity rate in Costa Rica (Fig. 1). Two networks (Observatorio Vulcanológico y Sismológico de Costa Rica, OVSICORI-UNA and Red Sismológica Nacional, RSN) have collected data in Costa Rica since the mid-1980s. Although both networks cover the same region, each network follows different ways of recording and treating the data and uses different velocity models for routine earthquake location. Previous seismological (Protti *et al.* 1994) and local earthquake tomography studies (Protti *et al.* 1996; Yao *et al.* 1999) show the great potential of seismological studies in this seismically and volcanically active subduction zone. Their results document the existence of low  $P$ -wave velocities beneath active volcanoes and the possible existence of a contortion in the subducting Cocos Plate, the Quesada Sharp Contortion (Figs 1 and 2). Inver-

sion of teleseismic arrival times observed at the OVSICORI-UNA network indicates the existence of a northeastward-dipping high-velocity body to depths of approximately 250 km beneath northern Costa Rica, interpreted as the subducting Cocos Plate (Colombo *et al.* 1997). The image of the subducting Cocos slab is less evident beneath central Costa Rica and no high velocities are observed beneath southern Costa Rica (Colombo *et al.* 1997). The previous local earthquake and teleseismic studies, however, are of low resolution owing to the lack of sufficiently large, high-quality data sets.

In this study we use a new high-quality data set of 3790 earthquakes giving 46 480  $P$ -wave observations to image the 3-D  $P$ -wave velocity structure beneath Costa Rica by local earthquake tomography. Our results confirm the existence of a steeply subducting

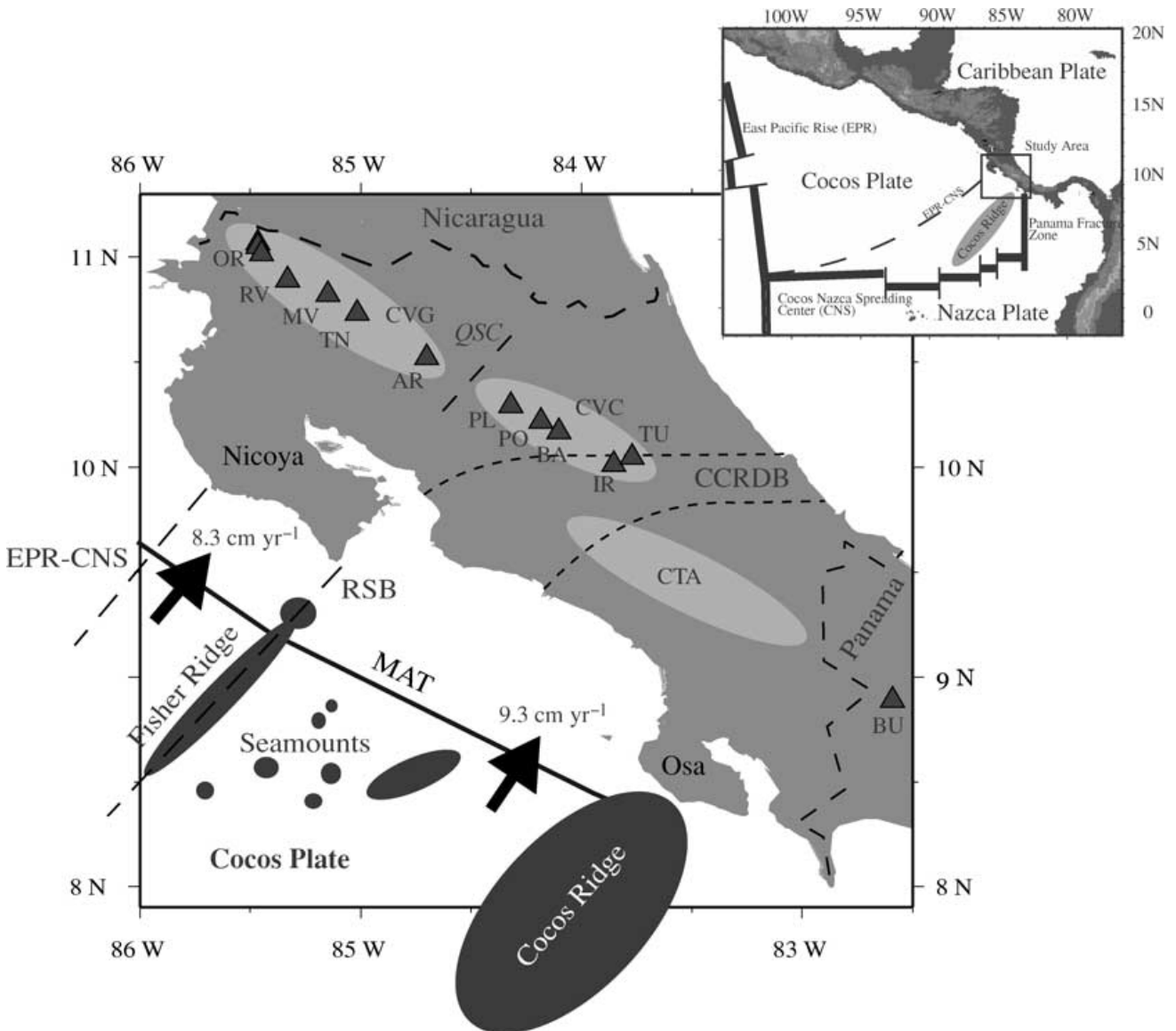


**Figure 2.** Significant tectonic features of the study area. EPR–CNS, boundary between oceanic crust formed at East Pacific Rise and Cocos–Nazca Spreading Center; RSB, rough–smooth boundary; MAT, Middle America Trench; CCRDB Central Costa Rica Deforming Belt; CVG, Cordillera Volcanica Guanacaste; CVC, Cordillera Volcanica Central; CTA, Cordillera de Talamanca; QSC, Quesada Sharp Contortion. Black triangles mark Quaternary volcanoes. OR, Orosi; RV, Rincon de la Vieja; MV, Miravalles; TN, Tenorio; AR, Arenal; PL, Platanar; PO, Poas; BA, Barba; IR, Irazu; TU, Turrialba; BU, Barú.

Cocos Plate beneath northern Costa Rica; beneath central Costa Rica, the maximum depth of the subducted Cocos Plate and associated Wadati–Benioff zone seismicity decreases gradually towards southern Costa Rica. Relocated intermediate-depth seismicity correlates well with predicted locations of hydrous metamorphic rocks, suggesting that dehydration plays a key role in generating intermediate-depth seismicity beneath central Costa Rica. We image large, low  $P$ -wave velocity areas within the lower crust beneath the southeasternmost volcanoes in central Costa Rica.

## TECTONIC SETTING

Costa Rica is located at the western margin of the Caribbean Plate (Fig. 2), an oceanic plateau formed during the Late Cretaceous as a result of the initial phase of a mantle plume that later formed the Galapagos hotspot (Duncan & Hargraves 1984; Sallares *et al.*

2001). Offshore Costa Rica, the Cocos Plate subducts beneath the Caribbean Plate along the Middle America Trench (MAT). The direction of convergence is  $025^{\circ}$ – $030^{\circ}$ , with subduction rates varying between  $8.3 \text{ cm yr}^{-1}$  in northwestern Costa Rica and  $9.3 \text{ cm yr}^{-1}$  in southeastern Costa Rica (De Mets 2001). Southeastern Costa Rica is part of the Panama block (Fig. 2) and forms the southern boundary of the Central Costa Rica Deformed Belt (CCRDB), a diffuse zone of active faulting across central Costa Rica (Fan *et al.* 1993; Goes *et al.* 1993; Marshall *et al.* 2000). The abundant seismicity (Fig. 1) in Costa Rica can be associated with subduction of the Cocos Plate beneath the Caribbean Plate, with internal deformation along the CCRDB, and with magmatic activity along the volcanoplutonic arc.

The oceanic lithosphere of the Cocos Plate was formed at the East Pacific Rise (EPR), at the present Cocos–Nazca Spreading system (CNS-3) and at its precursors CNS-2 and CNS-1 (Barckhausen *et al.* 1998, 2001). The boundary between oceanic crust formed at the EPR

and the CNS was long believed to be the ‘rough–smooth’ boundary formed by the Fisher seamount and the Fisher Ridge (Hey 1977). Recent work showed that the ‘rough–smooth’ boundary is located further north (Fig. 2) and corresponds to a narrow ridge offshore the central Nicoya Peninsula (Barckhausen *et al.* 2001). Oceanic crust formed at the EPR has an age of 24 Myr at the MAT (Barckhausen *et al.* 2001). Oceanic crust between the EPR–CNS boundary and the rough–smooth boundary (Fig. 2) formed at the CNS-1 and has a crustal age of 22.5 Myr (Barckhausen *et al.* 2001). The crust offshore central and southeastern Costa Rica (Fig. 2) formed at the CNS-2 and has crustal ages between 19 Ma in the north and 15 Ma in the south (Barckhausen *et al.* 2001).

Off Costa Rica, the Cocos Plate shows a remarkably variable morphology (Fig. 2) that can be divided into three segments (von Huene *et al.* 1995, 2000): (1) a smooth segment off north-eastern Costa Rica, (2) a seamount-dominated segment off central Costa Rica and (3) a Cocos Ridge segment off southeastern Costa Rica. The smooth segment is bounded by Fisher Seamount and Fisher Ridge to the south. At the trench, the crust breaks into normal faults trending subparallel to the axis of flexure (von Huene *et al.* 2000). The seamount-dominated segment is 40 per cent covered by seamounts (von Huene *et al.* 1995) and is bounded to the south by the subducting Cocos Ridge. Deep furrows and domes in the continental slope indicate seamount subduction (Ranero & von Huene 2000; von Huene *et al.* 2000). The Cocos Ridge off southeastern Costa Rica shows unusually thick oceanic crust (Stavenhagen *et al.* 1998; Walther *et al.* 2000) formed under the influence of the Galapagos hotspot during the Miocene. The thickness of the oceanic crust reaches 21 km along the crest of the ridge off Osa Peninsula (Walther *et al.* 2000). The MAT shallows to less than 1 km deep off the Osa Peninsula where the Cocos Ridge is subducting.

The Costa Rica volcanic arc (CRVA) is associated with the subduction of the Cocos Plate beneath the Caribbean Plate. It extends from Orosi volcano in northwestern Costa Rica to Turrialba volcano in central Costa Rica (Fig. 2). Southeastern Costa Rica shows a gap in the volcanic arc, which continues with the Baru volcano in northwestern Panama. The CRVA is traditionally divided into two cordilleras or mountain ranges (Fig. 2), the Cordillera Volcánica de Guanacaste (CVG) and the Cordillera Volcánica Central (CVC). The Cordillera de Guanacaste is a NW-trending chain of volcanoes that is offset 40 km southwest of the volcanic arc in Nicaragua (Weyl 1980). From NW to SE, the Quaternary volcanoes of the CVG are (Fig. 2): Orosí-Cacao, Rincón de la Vieja, Miravalles, Tenorio-Montezuma and Chato-Arenal. The volcanoes of the Cordillera de Guanacaste have geochemical signatures that are transitional between the depleted mantle source and a high subduction signal of the Nicaragua volcanoes and the enriched mantle source and low subduction signal of the central Costa Rica volcanoes (Carr & Stoiber 1990; Herrstrom *et al.* 1995). The Cordillera Central (Fig. 2) extends for approximately 80 km in central Costa Rica and consists of the Platanar-Porvenir, Poás, Barva, Irazú and Turrialba volcanoes; Turrialba volcano is offset 10 km north with respect to the other volcanoes of the Cordillera Central. The geochemical signature of the CVC is that of an ocean-island basalt with little influence by the subducting Cocos Plate (Carr & Stoiber 1990; Herrstrom *et al.* 1995). Active volcanism stopped 8 Ma in southeastern Costa Rica (Abratis & Woerner 2001) and a batholith of intermediate composition forms the Cordillera de Talamanca, which has been uplifted due to subduction of the Cocos Ridge (Kolarsky *et al.* 1995; Protti *et al.* 1996).

## LOCAL EARTHQUAKE TOMOGRAPHY

### Data and method

Local seismicity in Costa Rica is routinely recorded by two separate networks: OVSICORI-UNA and RSN. Both networks work independently and follow their own way of recording and treating data sets. They use different velocity models, different phase identifications and different quality assessments for routine earthquake location, complicating the use of a combined data set. Recently, these two data sets were merged into a clean phase data set for Costa Rica, encompassing 11 848 earthquakes (Fig. 1) and 132 331 *P*-wave observations in the period 1984–1997 (Quintero & Kissling 2001). The consistency and quality of the merged final data set were given priority over completeness. In the case of conflicting and suspicious information or when an apparent error in one of the original data sets could not be recovered, all data of this particular event were deleted. Using a subset of 822 well-locatable events, Quintero and Kissling (Quintero & Kissling 2001) calculated a minimum 1-D model for the Costa Rica region.

We selected 3790 earthquakes (Fig. 3) out of the merged data set by applying the following criteria: (1) greatest angle without observation (GAP) < 180°, (2) at least eight *P*-wave observations and (3) no large shifts (>10 km) during relocation with the minimum 1-D model. Our final data set encompasses 46 480 *P*-wave observations, giving an average of 12 *P*-wave observations per event. The station and earthquake density of our data set are high in central Costa Rica and low in northern and southern Costa Rica (Fig. 3). The majority of the earthquakes originate in the Wadati–Benioff zone (WBZ) of the subducting Cocos Plate with a maximum depth of 180 km beneath northern Costa Rica. Crustal seismicity beneath Costa Rica is also high owing to the North Panama Deformed Belt (NPDB), yielding a dense earthquake distribution down to 30 km depth (Fig. 3).

We used a damped, least-squared iterative solution (SIMULPS14) to solve the non-linear tomography problem (Thurber 1983; Eberhart-Phillips 1990; Haslinger & Kissling 2001). Hypocentre locations are included in the inversion as unknowns due to the coupling of hypocentre locations and velocities (Thurber 1992). Traveltimes through the velocity model are calculated using full 3-D shooting ray tracing (Virieux & Farra 1991; Haslinger & Kissling 2001). Other local earthquake tomography studies make use of *a priori* information in defining the plate interface as a first-order discontinuity and incorporating Snell’s law to bend rays along the dipping slab (e.g. Zhao *et al.* 1992, 1995; Nakajima *et al.* 2001). These approaches rely heavily on the quality of the *a priori* information since the dip of the slab is not adjusted during the inversion procedure. *A priori* information on the subducting Cocos Plate beneath Costa Rica, however, is not good enough to *a priori* define the geometry of the subducting Cocos Plate in the inversion.

Damping is a critical parameter in the inversion (Kissling *et al.* 2001) because damping affects both results and resolution estimates such as the diagonal element of the resolution matrix (RDE). High damping values yields low model perturbations and low RDE values feigning low resolution, whereas low damping yield high model perturbations and high RDE values feigning good resolution. Damping depends mainly on model parametrization and on the average observational error (*a priori* data variance) (Kissling *et al.* 2001) and can be determined by analysing trade-off curves between model variance and data variance for single-iteration inversions (Eberhart-Phillips 1986). Appropriate damping values show a significant decrease in

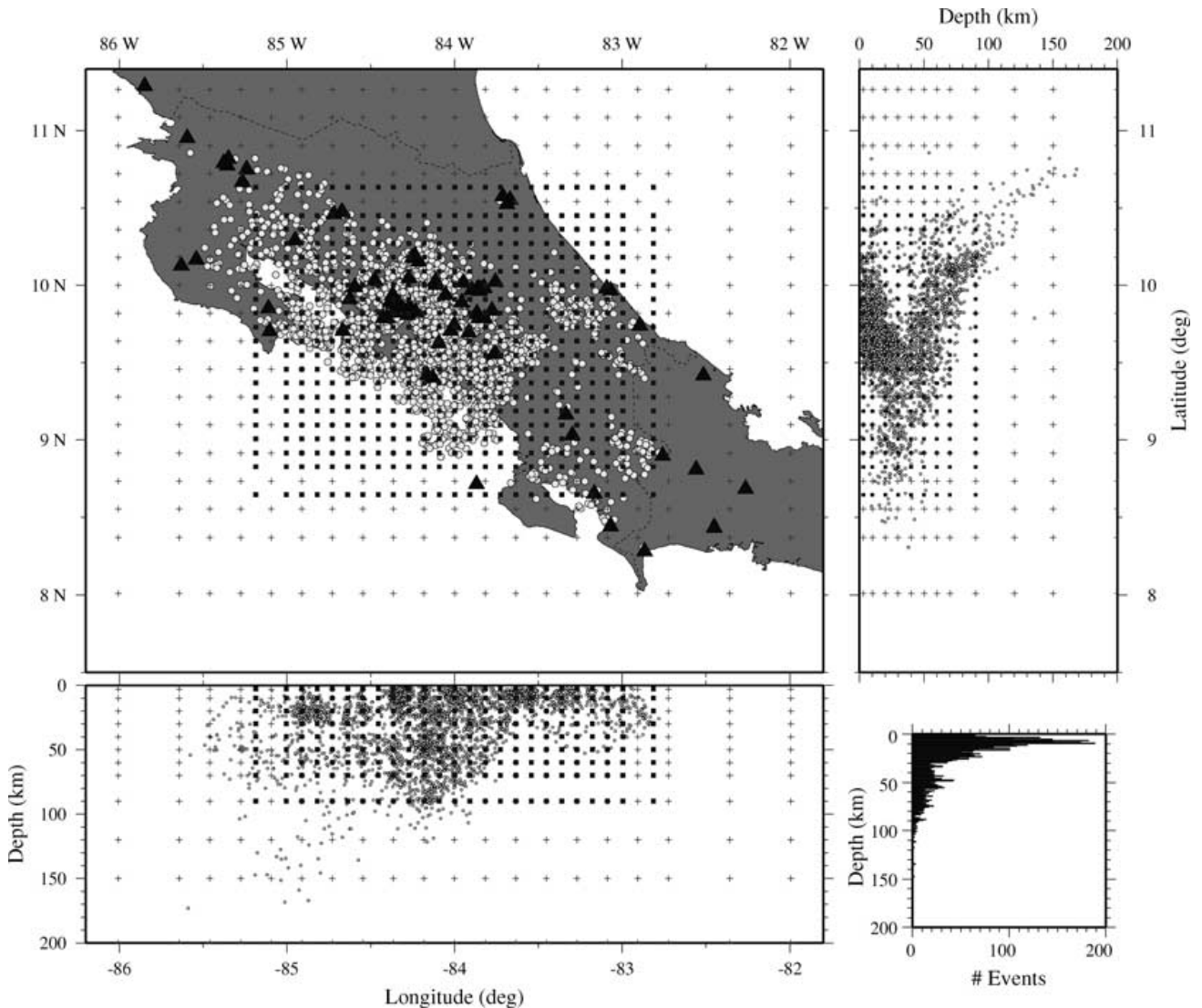


**Figure 3.** Hypocentre locations (dots), stations (black triangles), and grid nodes used in the inversion. Crosses and squares denote grid nodes of coarse- and fine-scale inversion, respectively. Bottom and upper right: projection of hypocentre locations and grid nodes on E–W and N–S cross-sections, respectively. Lower right: histogram of the hypocentre–depth distribution.

data variance without a strong increase in model variance, leading to the simplest model to fit the data. Fig. 4 displays such a trade-off curve for our data set. Initially, we did not invert for station delays, which resulted in a strong increase in data variance with decreasing damping (Fig. 4). Including station delays stabilized the inversion process in the sense that the data variance stayed nearly constant with decreasing damping. Station delays are usually introduced to compensate near-surface heterogeneities beneath the stations. This becomes more important as the heterogeneity of the velocity model increases as a result of lowered damping. In addition, our coarse spatial grid node spacing of 20 km and the high station density in central Costa Rica demanded station delays to decouple stations associated with the same grid node but having different near-surface geology. We finally selected a damping value of 500 that decreased data variance significantly without strongly increasing the model variance, thus yielding a smooth solution. Tests with synthetic data as described below showed either strongly decreased or strongly amplified amplitudes of the anomalies using damping values of 1000

and 100, respectively. A damping value of 200 would also be well suited, but we prefer to select a higher damping value to obtain the simplest model fitting the data.

The velocity model in SIMULPS14 is defined at grid nodes defined by intersecting lines in  $x$ -,  $y$ -,  $z$ -directions. Velocities are linearly interpolated between the grid nodes and no further smoothing constraints are applied. Model parametrization in seismic tomography must account for *a priori* knowledge of Earth's structure and the resolution capability of the available data set (Kissling *et al.* 2001). In the extreme case, this trade-off can lead to a dense grid spacing being required to adequately represent *a priori* known structures such as sedimentary basins or Moho topography, but on the other hand coarse-grid spacing is required by non-uniform ray coverage. Uneven grid spacing is often used to account for this trade-off (Abers & Roecker 1991; Bijwaard *et al.* 1998) but very unevenly spaced models complicate the interpretation of tomographic results and solution quality. Velocity changes associated with changes in grid spacing, for example, may be interpreted as false geological boundaries.

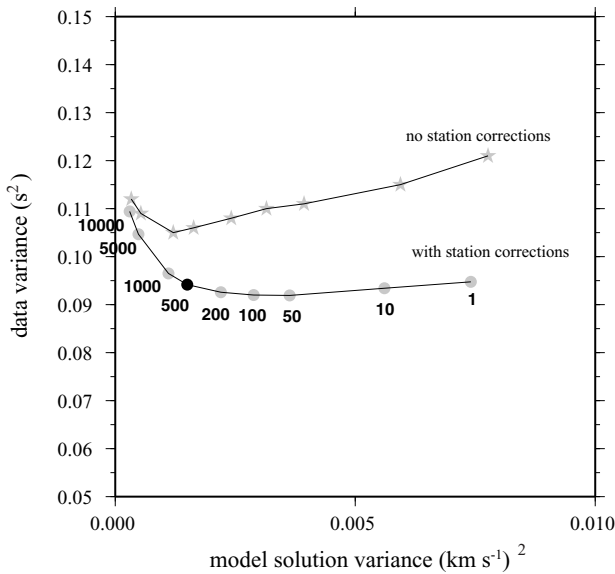


**Figure 4.** Trade-off curves to determine damping parameter. Grey stars and grey circles denote inversion without and with station corrections, respectively. Selected damping parameter of 500 is shown by black circle.

Assessing the appropriate model parametrization is complicated by the fact that resolution estimates are strongly affected by the chosen model parametrization (Kissling *et al.* 2001). Coarse grid spacing yields large resolution estimates, whereas fine-grid spacing yields low resolution estimates. The station and earthquake distribution is very heterogeneous in our study (Fig. 3). A high number of stations and earthquakes would allow for fine-grid node spacing in central Costa Rica, whereas the station and earthquake distribution is sparse in the remaining parts, demanding a large grid node spacing. To overcome this problem we first inverted for a coarse regional velocity model and subsequently used a subset of 2924 earthquakes comprising 30 174 *P*-wave observations to invert for a fine-scale, detailed velocity model of central Costa Rica (Fig. 5). Initial veloci-

ties of the fine-scale inversion are taken from the results of the coarse velocity model linearly interpolated on to the fine-grid node spacing. Only stations and earthquakes, which hypocentre locations were obtained by the coarse-scale inversion, inside the subvolume were used for this fine-scale inversion. To present the final results, both velocity models are combined into one model (Fig. 5). This series of inversions with increasing complexity guarantees a smooth velocity model throughout the entire volume without artificially introduced heterogeneities due to uneven grid spacing (Eberhart-Phillips 1990; Husen *et al.* 2000). We chose a model parametrization of  $20 \times 20$  km<sup>2</sup> horizontally for the coarse regional model (Fig. 3). This model parametrization represents the finest possible model grid spacing without showing a strongly heterogeneous pattern of the derivative weighted sum (DWS) (Fig. 6), a measure for the ray density (Husen *et al.* 2000). Grid node spacing with depth varies between 7 km at shallow depth (<10 km), 10 km at intermediate depth (<70 km) and 20 km at greater depth (>70 km) (Fig. 3). The same grid node spacing with depth was used for the fine-scale inversion in central Costa Rica, but horizontal grid node spacing was reduced to  $10 \times 10$  km<sup>2</sup> (Fig. 3).

Linearization of the non-linear 3-D inversion problem demands initial velocities and hypocentre locations close to their true values. We chose the minimum 1-D model of Quintero & Kissling (2001) as an initial reference model for the coarse regional inversion as it has proven to be the most appropriate initial reference model in local earthquake tomography (Kissling *et al.* 1994). Velocities of the minimum 1-D model were interpolated at depth to match the gradient formulation used in SIMULPS14. Initial hypocentre locations were obtained by relocating the selected data set using the minimum 1-D model including station delays. Velocities and hypocentre locations of the coarse regional model were used as initial values for the fine-scale inversion in central Costa Rica. Initial runs of the coarse-scale inversion showed a large reduction in data variance of 25 per cent just by relocating hypocentre locations prior to the inversion for velocities. Hypocentre locations were shifted on average systematically by 1.5 km in epicentre and 2 km in depth. This indicates that the hypocentre locations depend strongly on the station delays of the minimum 1-D model, which were initially set to zero

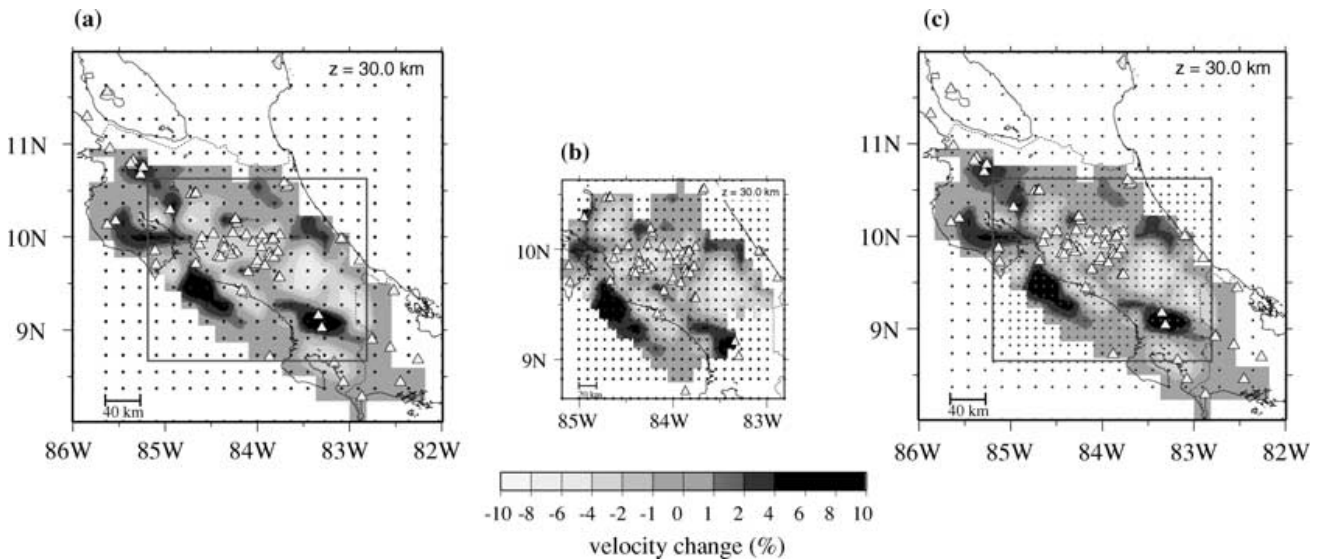


**Figure 5.** Tomographic results at a depth of 30.0 km obtained by gradual inversion scheme used in this study. (a) Coarse-scale model ( $20 \times 20$  km<sup>2</sup>), (b) Fine-scale model ( $10 \times 10$  km<sup>2</sup>) for central Costa Rica, (c) combined model. Initial hypocentre locations and initial velocities for fine-scale inversion are taken from the coarse-scale model. See the text for further details.

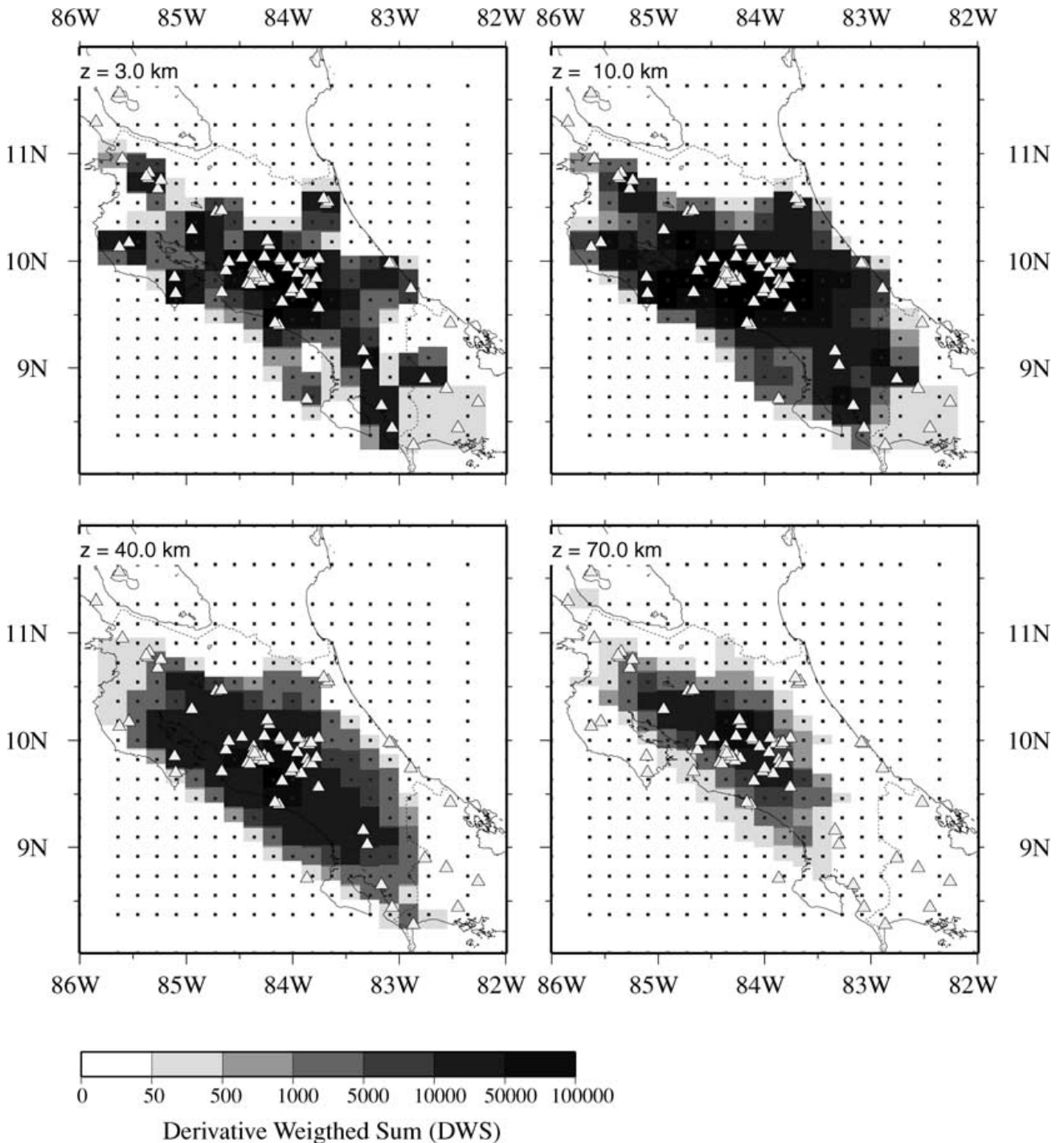


**Figure 6.** Derivative weighted sum displayed in horizontal planes at different depths indicated. Dark shading indicates a high ray density. White triangles and squares denote stations and grid nodes of the inversion, respectively.

in the inversion. Station delays of the minimum 1-D model account for near-surface heterogeneities at a station and large-scale velocity heterogeneities such as a dipping slab (Kissling 1988; Husen *et al.* 1999). Setting these station delays to zero while relocating the events in the 1-D velocity model can result in systematic shifts in the hypocentre locations. To solve this problem, we decided to fix the hypocentre locations during the first iteration; in the following iterations hypocentre locations are always updated after each

velocity inversion. Following this approach yields identical results but slightly increased amplitudes compared with results obtained by relocating the events within the first iteration (Fig. 7). The coarse regional inversion reduced data variance by 55 per cent compared with the 1-D starting model. The additional fine-scale inversion achieved another 33 per cent reduction in data variance. The final root mean square (rms) over all traveltimes residuals is 0.246 s after the fine-scale inversion. This relatively high rms may reflect unmodelled

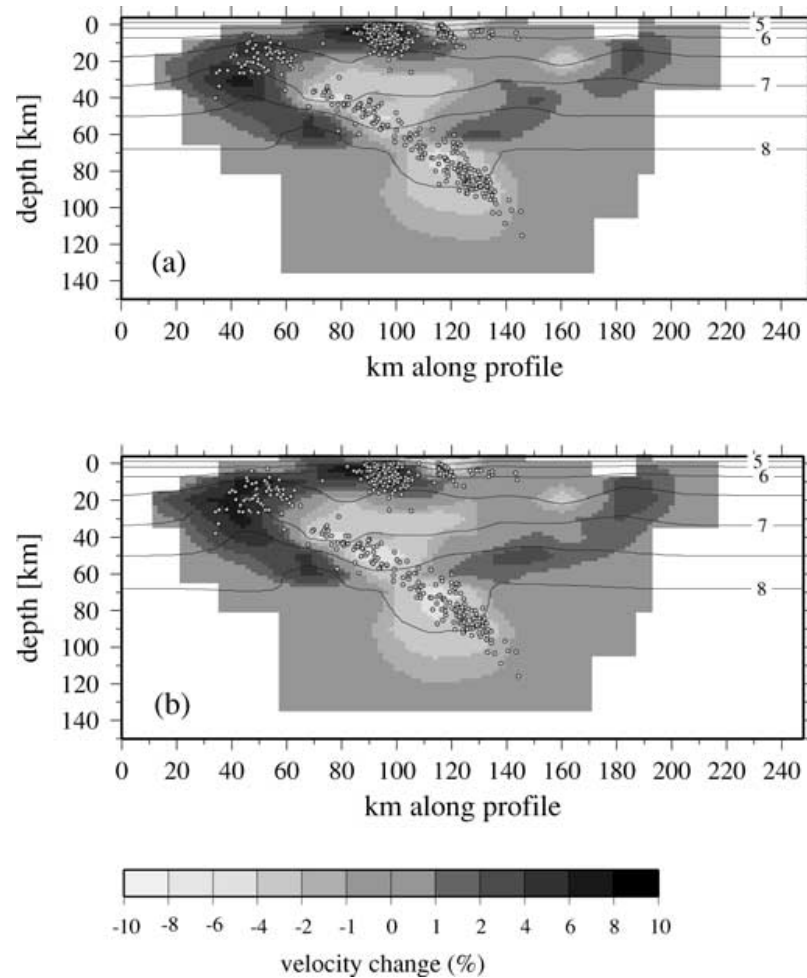


**Figure 7.** Comparison of tomographic results along cross-section C–C' (see Fig. 12 for locations). Results were obtained by either (a) relocating earthquakes within the 1-D initial reference model prior to first iteration or (b) fixing earthquake locations prior to first iteration. See the text for further details.

velocity variations and/or high picking errors since many different people picked this data set.

### Solution quality

During the inversion process unrealistic model perturbations (artefacts) may be introduced in areas of low resolution or even in areas of good resolution. A careful assessment of the solution quality is required to define areas of low resolution and to detect possible artefacts. In principle, the resolution of a certain volume depends mainly on the geometrical distribution and density of rays (ray coverage). Several techniques exist (e.g. Reyners *et al.* 1998; Husen *et al.* 2000) to assess ray coverage, including resolution estimates such as the hit count, diagonal element of the resolution matrix (RDE), the spread function and tests with synthetic data such as checkerboard tests (Humphreys & Clayton 1988; Zelt 1998) and restoring resolution tests (Zhao *et al.* 1992). We performed the following analyses and tests for both the coarse- and the fine-scale inversions. For reasons of brevity we will only present the results for the coarse inversion, but results were similar for the fine-scale inversion.

Tests with synthetic data can provide useful information concerning model parametrization, damping and solution quality (Kissling *et al.* 2001). Checkerboard tests are commonly used to assess solu-

tion quality because they are intuitive. However, checkerboard tests give only good estimates of the amount of smearing. The ability of the data to resolve a fine-scale structure such as a checkerboard does not imply that large-scale structures are resolved as well (Leveque *et al.* 1993). Restoring resolution tests use the obtained inversion results as an input model to calculate synthetic traveltimes (Zhao *et al.* 1992). This possesses the drawback that areas of low resolution are identified as areas of good resolution due to the good recovery of the input model, which either shows low-amplitude anomalies or even artefacts in areas of low resolution. Following Haslinger *et al.* (1999) and Husen *et al.* (2000), we designed a synthetic model, called the characteristic model that is based on the inversion results obtained with 'real' data. A characteristic model retains the sizes and amplitudes (characteristics) of anomalies seen in the inversion results but has different shapes and different signs for the anomalies. For crustal layers (<30.0 km depth), our 'real' tomographic results show a complicated pattern with many different anomalies varying in size and shape. At greater depth the anomaly pattern smooths and only a few large anomalies are observed. These characteristics are taken into account in the synthetic model by many anomalies of varying size and shape in the crustal layers and fewer and larger anomalies at greater depth (Fig. 8). Synthetic traveltimes through the characteristic

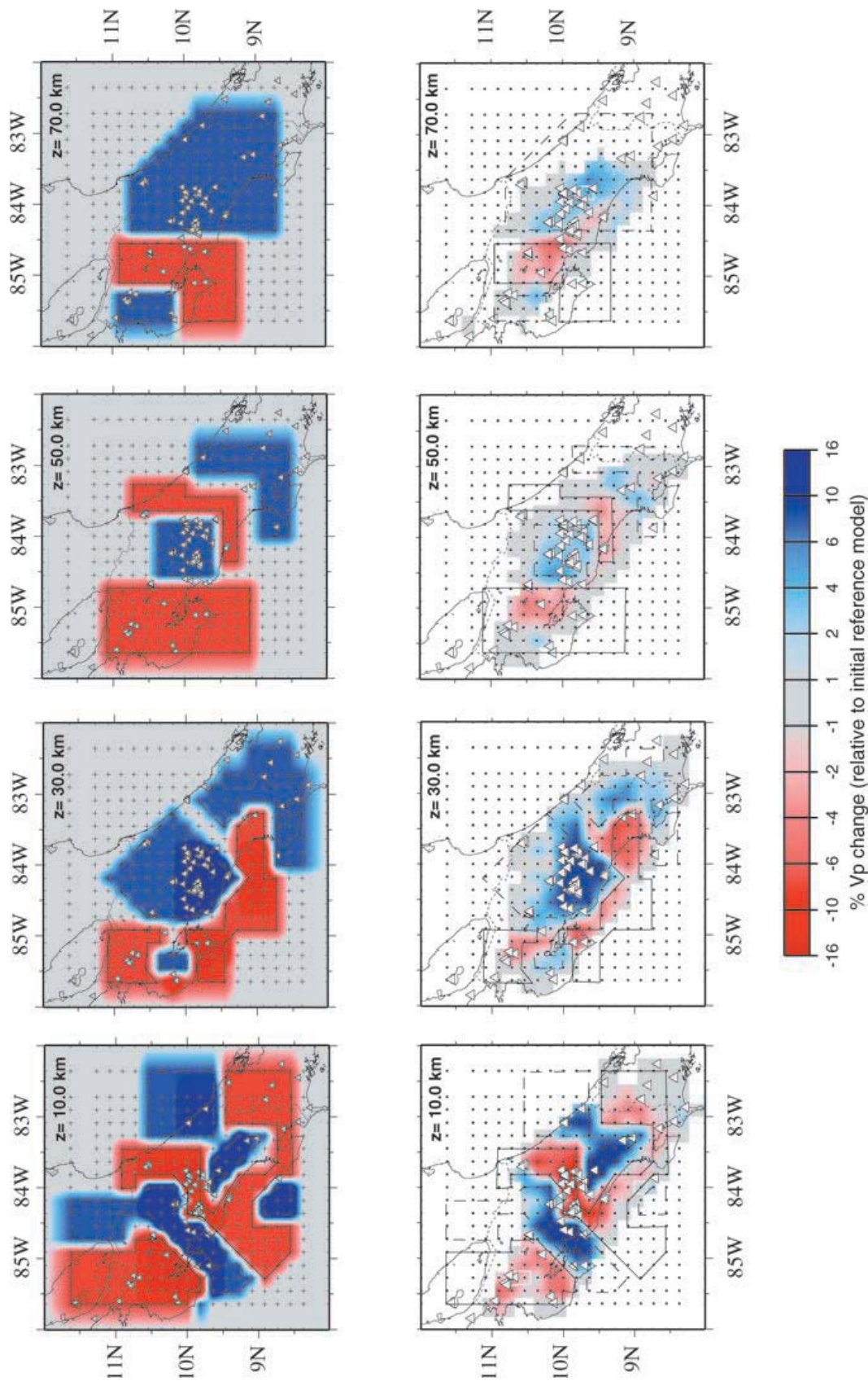


**Figure 8.** Assessment of solution quality by test with synthetic data. Top: synthetic input model; bottom: recovered model after inversion.  $P$ -wave velocity perturbations are shown relative to the 1-D initial reference model. Horizontal views are shown for different indicated depths. Black lines denote the position of anomalies in the synthetic input model. White triangles denote stations used in the inversion. See the text for a more detailed description of synthetic data tests.

model were calculated using a finite-difference solution to the eikonal equations (Podvin & Lecomte 1991) for the source–receiver distribution of the real data set. Gaussian-distributed noise was added with a standard deviation proportional to the original observational weight. Inversion of synthetic traveltimes uses the same inversion parameters (model parametrization, damping, number of iterations) as the inversion of the ‘real’ data. By comparing inversion results using synthetic traveltimes to the synthetic input model (Fig. 8) we identify areas of good and low resolution, i.e. good and poor recovery of the input model. Central Costa Rica is well resolved down to 70 km depth. Because of the lack of seismicity and stations, the southern part of Costa Rica is only well resolved down to 30 km depth. At 70 km depth the leakage of low velocities into areas of high-velocity indicates resolution problems due to rays originating in the WBZ beneath central Costa Rica and travelling to stations in southern Costa Rica (Fig. 8). Northern Costa Rica is well resolved down to a depth of 30 km (Fig. 8). The lack of stations in northern Costa Rica inhibits any resolution along the border between Costa Rica and Nicaragua. The good recovery of the sign and geometry of the anomalies and the homogenous distribution of DWS (Fig. 6) validate our chosen model parametrization. Damping of the solution results in decreased amplitudes of the recovered anomalies compared with the amplitudes of the input model. Crustal layers show an amplitude decrease of 30–40 per cent, whereas deeper layers show a decrease of >50 per cent. A lower damping value would increase the amplitude recovery but stronger smearing effects would hamper the overall picture.

SIMULPS14 computes the full resolution matrix and diagonal elements of the resolution matrix are shown in Fig. 9 for three vertical cross-sections. The diagonal element of the resolution matrix (RDE) is often used to assess the resolution or solution quality. Theoretically, a perfect resolution is indicated with a RDE of 1, but the RDE depends strongly on damping and model parametrization, complicating its use for resolution assessment. We only found a high RDE (>0.8) for a few model parameters in the topmost layers (Fig. 9). With increasing depth, the RDE values decrease to 0.1–0.3 owing to diminishing ray coverage (Fig. 9). In comparison with the results using synthetic data (Fig. 8), however, these low RDE values still indicate a reliable solution. Off-diagonal elements in the resolution matrix contain information on how much the solution of a model parameter depends on its neighbours, i.e. how much smearing is involved. This information can be assessed by computing the spread function, which compresses each row of the resolution matrix into a single number (Toomey & Foulger 1989; Michelini & McEvelly 1991). The smaller this number the more independent or peaked is the solution. However, absolute values of the spread function depend on damping and model parametrization in the same way that the RDE does. In addition, the spread function does not indicate the direction of smearing. This could be shown by plotting the entire row of a resolution matrix (Toomey & Foulger 1989; Husen *et al.* 2000) for each model parameter, but this becomes impractical for thousands of model parameters. Reyners *et al.* (1998) introduced smearing or resolution contours to visualize the direction of smearing in 2-D cross-sections. Fig. 9 displays such smearing contours for vertical cross-sections. Smearing contours in Fig. 9 outline those regions where the off-diagonal elements are still 70 per cent of the corresponding diagonal element. Significant smearing occurs only at those model parameters located at the edge of the model (Fig. 9). As can be inferred from Fig. 9, only model parameters with a RDE <0.1 show large smearing contours. In combination with the results of the test with synthetic data we consequently define areas of good resolution as those showing a RDE >0.1.

## TOMOGRAPHIC RESULTS

We present our tomographic images in a series of horizontal depth sections at different depths and vertical depth sections parallel to the strike of the subducting Cocos Plate (Figs 10 and 11). We focus only on anomalies associated with the subducting Cocos slab and active volcanism. Horizontal and vertical depth sections are drawn through the merged velocity model that combines the results of the coarse- and fine-scale inversions. Velocity perturbations relative to the minimum 1-D model are shown with red to blue colours and absolute velocities are shown with contour lines (Fig. 11). We choose to show velocity perturbations as primary results because variations in the physical state of the rocks such as temperature or the presence of fluids are more easily seen. Nevertheless, we show absolute velocities by contour lines to facilitate interpretation. Hypocentre locations of those events used in the coarse- and fine-scale inversions are obtained by relocating them in the merged 3-D velocity model. Hypocentre locations are shown for each profile within 10 km perpendicular to the profile (Fig. 11).

WBZ seismicity shows a gradual decrease in maximum depth from northwest to southeast (Figs 11 and 12). The deepest events (>140 km depth) are found along the border between Nicaragua and Costa Rica. The shallowest depth of the WBZ seismicity (<40 km depth) is in southeastern Costa Rica where interaction with the Cocos Ridge occurs and active volcanism stops. As can be inferred from Figs 11 and 12, WBZ seismicity is sparser in northwestern and southeastern Costa Rica than in central Costa Rica. In part this may reflect our selection criterion that requires at least eight *P*-wave observations. The lower number of stations in northwestern and southeastern Costa Rica also yield a lower number of usable events.

Our tomographic images reflect the complexity of the subducting Cocos Plate beneath Costa Rica. Along the northernmost profile, A–A' (Figs 11a and b), the Cocos Plate represents the oldest part of the lithosphere formed at the Cocos–Nazca spreading centre. The seafloor topography is smooth (von Huene *et al.* 2000) and magnetic anomalies suggest a crustal age of 24 Ma (Barckhausen *et al.* 2001). We image the subducting Cocos Plate as a high-velocity feature down to 70 km depth (Fig. 11a); resolution below 70 km depth is poor. The most remarkable feature is a zone of low velocities paralleling the top of the subducting Cocos Plate down to 30 km depth (Fig. 11a). A small low-velocity zone is observed beneath Rincon de la Vieja volcano at 20 km depth, but poor resolution means it may not be reliable.

Profile B–B' (Figs 11c and d) runs along the proposed Quesada Sharp Contortion (QSC) (Protti *et al.* 1994). The seafloor topography shows a large seamount, Fisher Seamount, followed by the Fisher Ridge in front of the trench (Fig. 12). Fisher Seamount and Fisher Ridge are interpreted as representing a propagator, a bathymetric feature persistent for at least the last 20 Myr (Barckhausen *et al.* 2001). Except for the low-velocity zone at 30 km depth, we image the subducting Cocos Plate as a high-velocity feature down to 90 km depth (Fig. 11c); at greater depth, low velocities replace the observed high velocities, but resolution is poor. Most of the WBZ seismicity is located within the high-velocity areas except for a few events beneath 90 km depth, which are in the zone of low velocities (Figs 11c and d). High velocities at depths below 40 km extend beneath the active volcanic arc, where we expect the mantle wedge. A broad zone of low crustal velocities is observed directly beneath Arenal volcano (Fig. 11c). No seismicity is observed within this zone of low velocities (Fig. 11d).

Profiles C–C' and D–D' lie in the seamount-dominated segment of the Cocos Plate (Fig. 12), a segment 40 per cent covered by

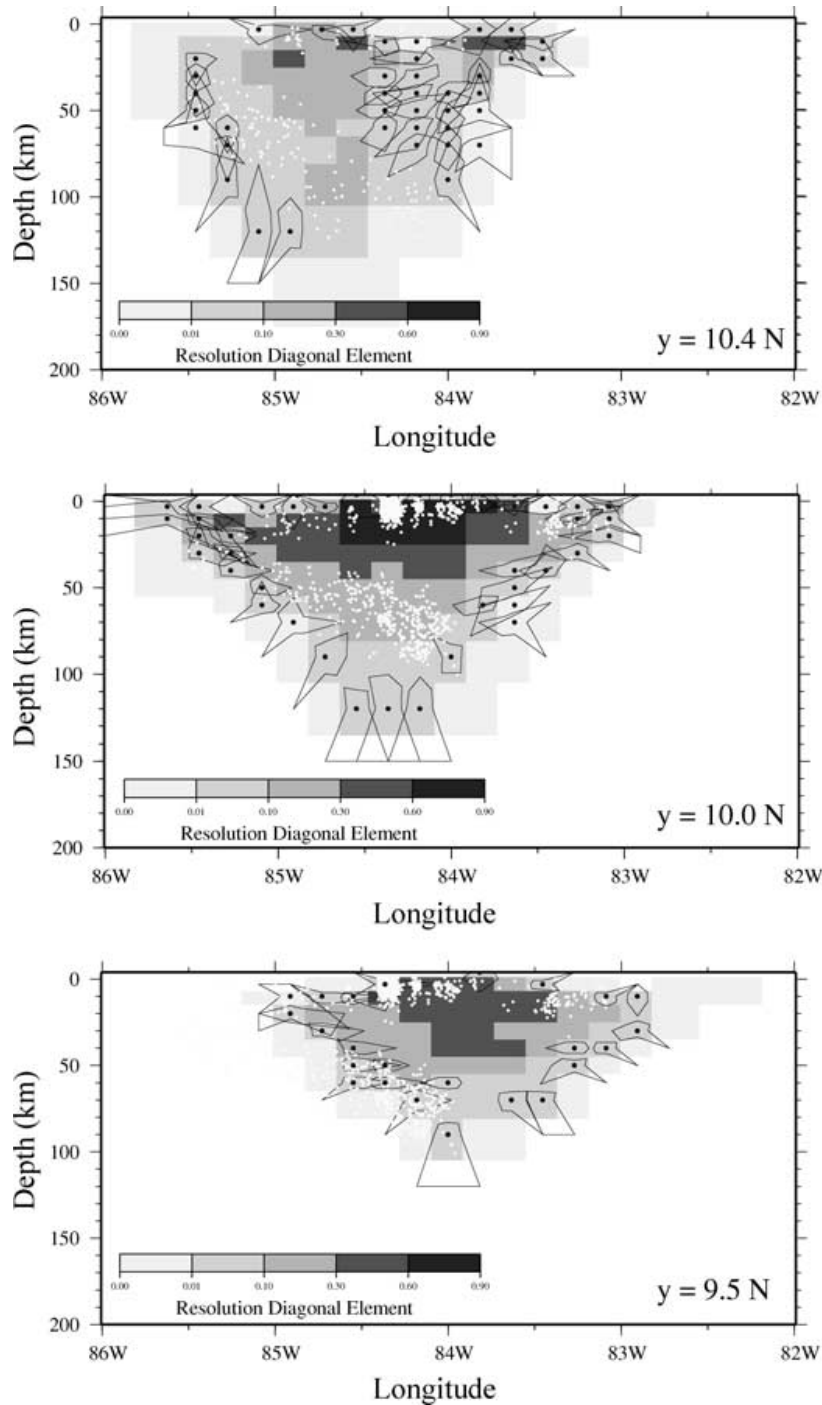


**Figure 9.** Diagonal element of the resolution matrix displayed at three different vertical cross-sections along constant latitude as indicated. Superimposed are 70 per cent resolution contours, depicting possible smearing effects. Resolution contours are only shown for grid nodes with significant smearing. White dots denote earthquakes. Earthquakes are only plotted within  $\pm 5$  km of the plane depth as indicated.

seamounts (von Huene *et al.* 2000). The ages of the Cocos Plate at the trench vary between 19 Myr along profile C–C' and 18 Myr along profile D–D' (Barckhausen *et al.* 2001). Although subduction parameters do not differ significantly, these two profiles show remarkable differences in their tomographic images (Figs 11e and g). Along both profiles we image the subducting Cocos Plate as a high-velocity feature down to 60 km depth, at which

level low velocities appear. However, along profile C–C' these low velocities extend updip parallel to the Cocos Plate to 30 km depth (Fig. 11e), whereas along profile D–D' the low velocities are restricted to  $>60$  km depth except for a small zone of low velocities at 30 km depth beneath the coast (Fig. 11g). A large area of low crustal velocities is observed beneath Irazu and Turrialba volcanoes along profile D–D'. This zone narrows at shallow depth

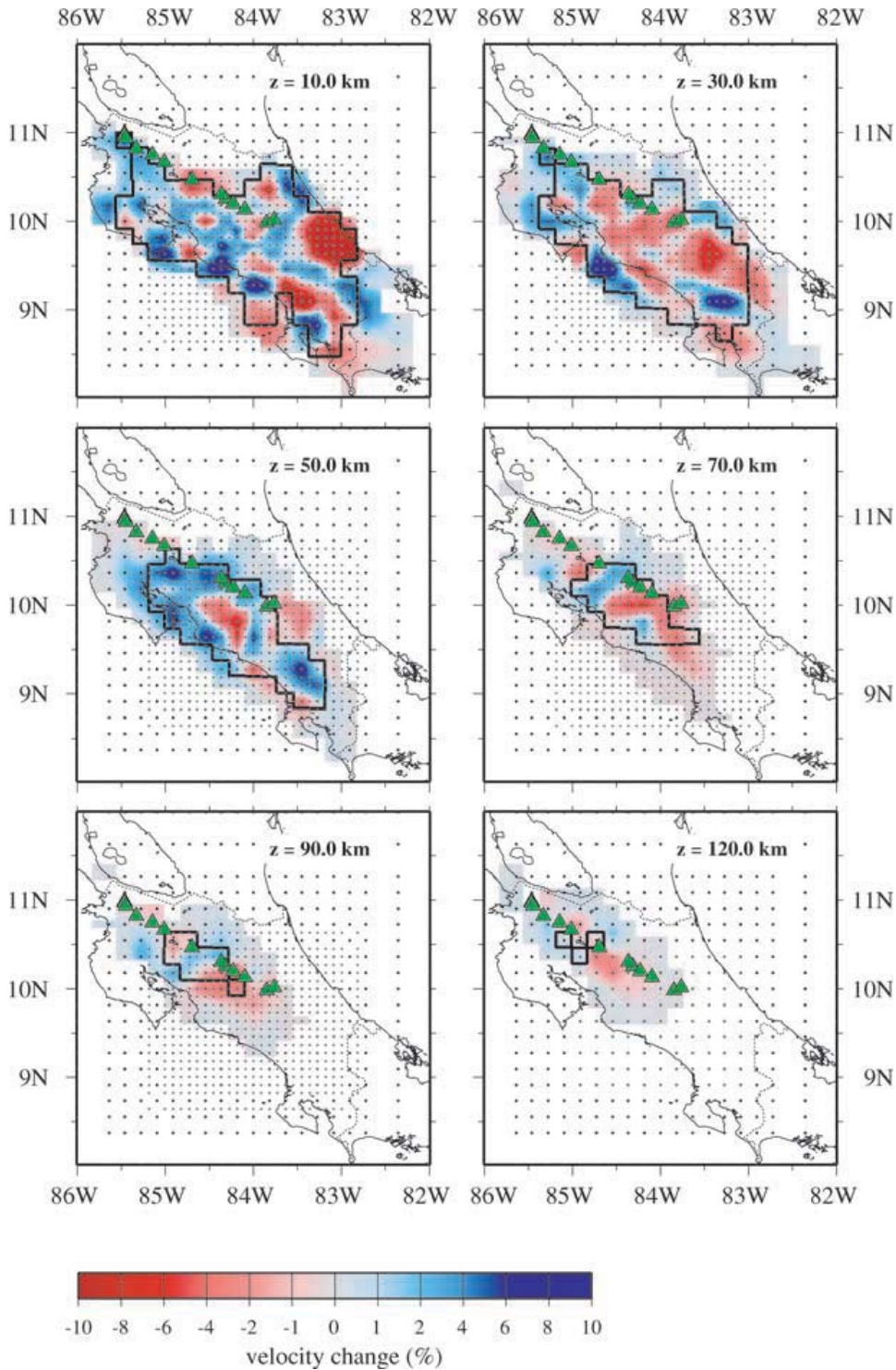


**Figure 10.** Horizontal depth sections through the final  $P$ -wave velocity model at different depths as indicated. Velocity perturbations are shown relative to 1-D initial reference model. Black contour line marks boundary between well and fairly well-resolved areas. Anomalies outside well-resolved areas should only be interpreted if they extend over several grid nodes. Grid nodes of the coarse- and fine-scale inversion are shown by dark and grey dots, respectively. Green triangles mark active volcanoes.

and extends directly beneath the volcanoes (Fig. 11g). Along profile C–C' a similar zone of low velocities is observed beneath Poas volcano, but it is located trenchward of the volcano (Fig. 11e). There is no connection between the low-velocity zone at depth

and the low-velocity zone directly beneath the volcano. The WBZ seismicity along profile C–C' is located mostly within the 10 km thick zone of low velocities (Figs 11e and f), and the maximum depth of seismicity is 120 km, whereas the WBZ seismicity along

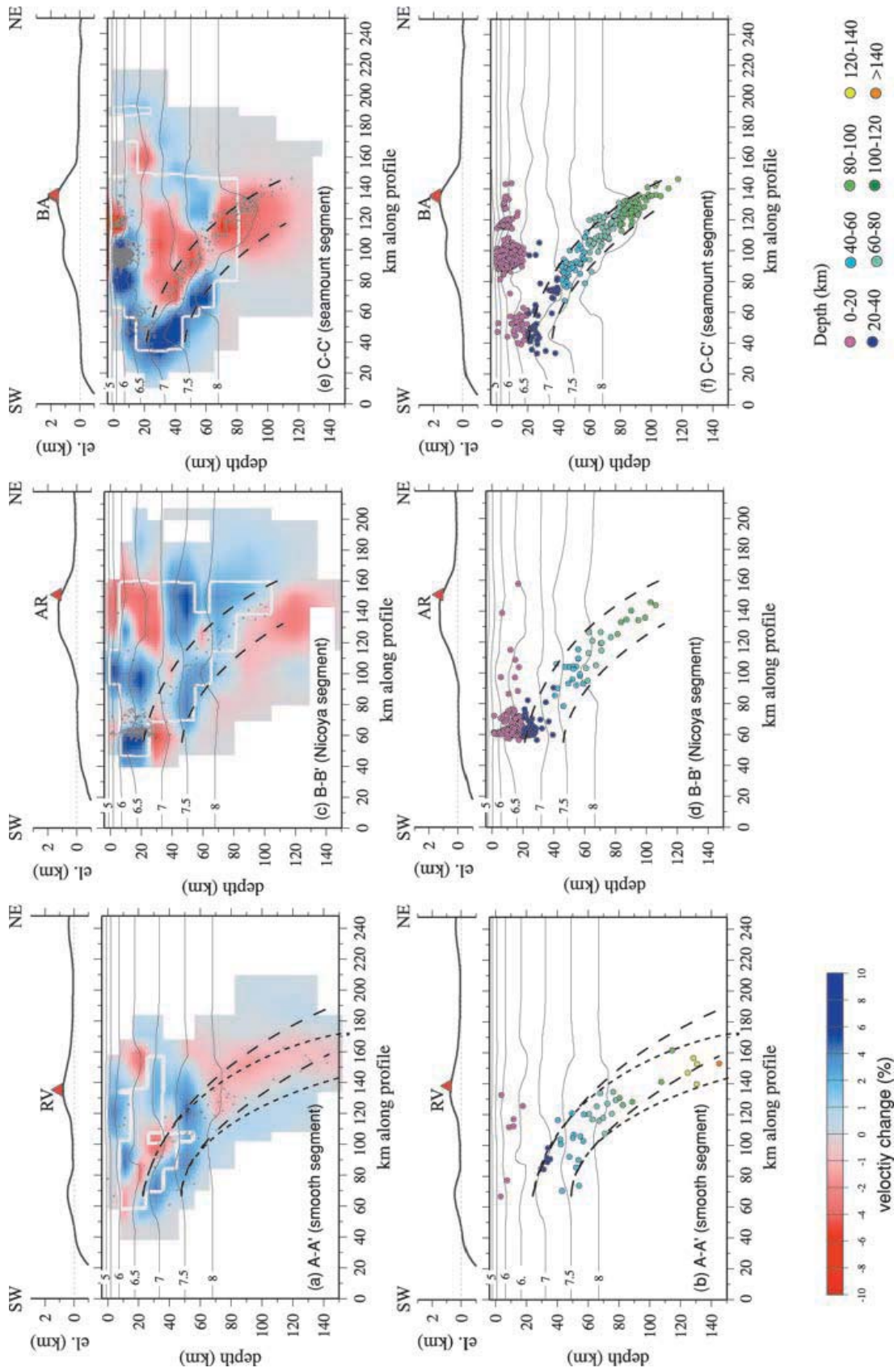


**Figure 11.** Vertical depth sections parallel to the dip of the subducting Cocos Plate of the 3-D  $V_p$  model (top) and seismicity (bottom), respectively. Velocity perturbations are shown relative to 1-D initial reference model. White contour line marks boundary between well and fairly well resolved areas. Anomalies outside well resolved area should only be interpreted if they extend over several grid nodes. Contour lines mark absolute  $P$ -wave velocities; the contour interval is  $0.5 \text{ km s}^{-1}$ . Hypocentre locations are projected within  $\pm 10 \text{ km}$  perpendicular to the profile. The depth is colour coded as indicated. Dashed lines mark the envelope of the WBZ seismicity. On top of each cross-section the corresponding topography is shown. Red triangles mark Quaternary volcanoes. RV, Rincon de la Vieja; AR, Arenal; BA, Barba; IR, Irazu; TU, Turrialba; CT, Cordillera de la Talamanca; OP, Osa Peninsula.

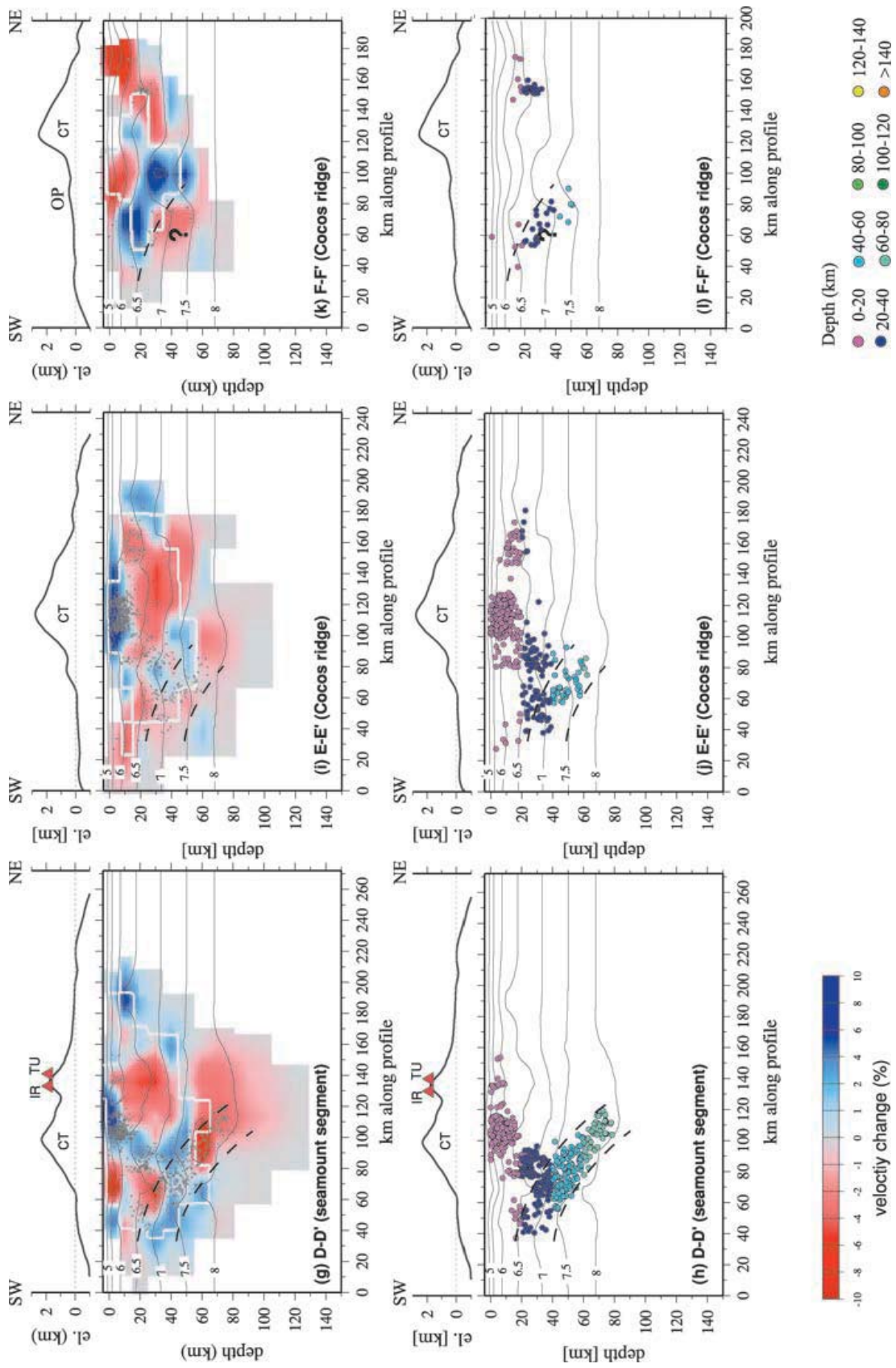
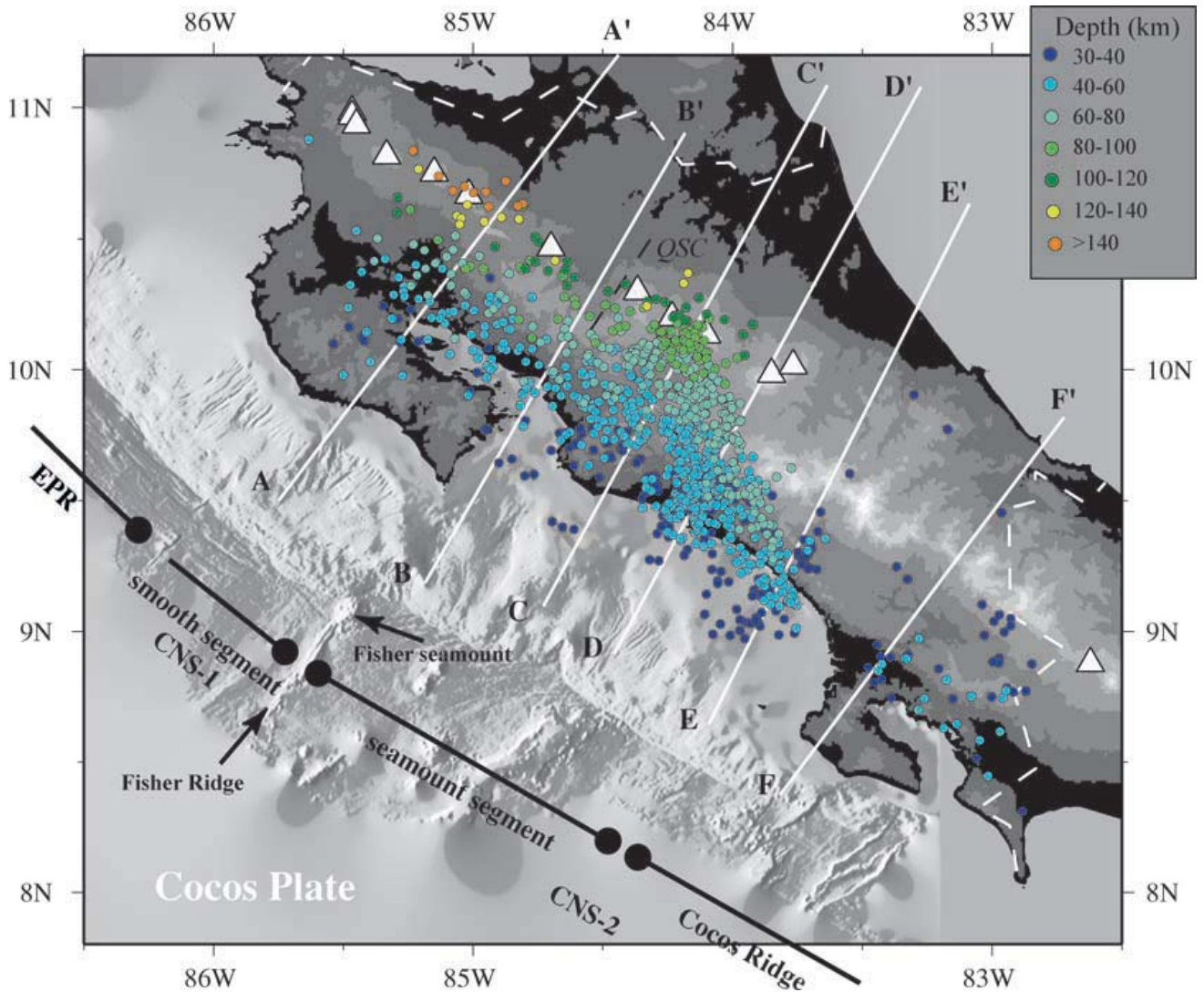


Figure 11. (Continued.)



**Figure 12.** Epicentres of Wadati–Benioff seismicity for earthquakes with focal depths  $>30$  km. Only well-locatable earthquakes used in the 3-D inversion are shown. Different depth ranges are colour coded as indicated. White lines denote the location of vertical cross-sections shown in Fig. 11. White triangles mark Quaternary volcanoes. See Fig. 1 for an explanation of the main offshore tectonic features. The dashed line marks the location of the proposed Quesada Sharp Contortion (QSC) (Protti *et al.* 1994).

profile D–D' forms a more diffuse 20 km wide band that extends only down to 80 km depth (Figs 11g and h). No seismicity is observed within the large low-velocity zones beneath the volcanoes except for shallow seismicity directly beneath the volcanoes.

Profiles E–E' and F–F' run along the Cocos Ridge (Fig. 12). The Cocos Ridge forms a 1.5 km high broad swell above the seafloor and is interpreted as a hotspot trace formed as the Cocos Plate passed over the Galapagos hotspot during the Miocene (Hey 1977). The age of the Cocos ridge at the trench is 15–16 Ma (Barckhausen *et al.* 2001), thus representing the youngest oceanic lithosphere in our study area. The oceanic crust of the Cocos ridge is extremely thick, 21 km off the Osa Peninsula (Walther *et al.* 2000) along profile F–F' and 12 km along profile E–E' (Stavnhagen *et al.* 1998). The subducting Cocos Plate is not imaged as a high-velocity feature along profile E–E' and F–F' but by low velocities. These low

velocities may represent warm oceanic lithosphere due to its unusual thickness and young age. Along profile E–E' a diffuse WBZ terminates at 60 km depth. No clear WBZ exists along profile F–F', and seismicity stops at 40 km depth (Figs 11j and l). A large area of low velocities is observed beneath the Cordillera Talamanca along profile E–E' (Fig. 11i) and have been interpreted as a low-density remnant of an earlier phase of magmatism associated with the Talamanca batholiths (Protti *et al.* 1996). Along profile F–F' low velocities and seismicity associated with the subduction of Cocos ridge terminate against a body of high velocities (Fig. 11k). These high velocities may represent part of the Panama block (the Cretaceous Chorotega and Choco oceanic basement terranes, Marshall *et al.* 2000) that stretches from Panama into central Costa Rica. As can be inferred from our tomographic image, the Panama block may form some sort of backstop that terminates shallow subduction of the Cocos ridge.

## DISCUSSION

## Structure of the subducting Cocos Plate

In general, subducting oceanic slabs are imaged by seismic tomography as high- $V_p$  features (Zhao *et al.* 1995; Reyners *et al.* 1998; Husen *et al.* 2000; Zhao *et al.* 2000; Nakajima *et al.* 2001). After formation, mid-ocean ridge lithosphere cools and thickens until it is subducted. Subduction rates are generally faster than thermal diffusion, yielding a cold core within the subducting slab and a strong temperature gradient across the interface between the subducting plate and the overlying plate. The temperature difference between the cold slab and the warm surrounding mantle depends mainly on the age of the subducting plate and the subduction rate. The older the plate and the faster the subduction, the colder the subducting slab. The colder the slab, the higher the velocity difference between the subducting slab and the surrounding plate. To first order, our tomographic images show a NE-dipping high-velocity anomaly that is consistent with the cold subducting Cocos Plate (Fig. 11).

In central Costa Rica, we lose track of the high-velocity slab at depths greater than 60–70 km (profiles C–C' and D–D'), where the expected high velocities are replaced by lower velocities (Figs 11e and g). These low velocities extend updip along profile C–C' parallel to the high-velocity slab (Fig. 11e). In particular, along profile C–C' nearly all of the WBZ seismicity at that depth is located within the low-velocity zone. This observation supports the growing evidence that the simple picture of a cold, dense subducting slab is oversimplified. During subduction, oceanic lithosphere undergoes phase transformations, including dehydration reactions (Peacock 1990, 1996). We computed the equilibrium mineralogy of the subducting Cocos Plate for northern and central Costa Rica using the method of Hacker (1996) and Hacker *et al.* (2003a) (Fig. 13). Our computations are based on thermal models assuming a slab age of 30 Myr in northern Costa Rica and 20 Myr in central Costa Rica, respectively (Hacker *et al.* 2003b). The subduction rates are 83 mm yr<sup>-1</sup> for northern Costa Rica and 87 mm yr<sup>-1</sup> for central Costa Rica, respectively. The subducting oceanic crust was modelled as a mid-

ocean ridge basalt + H<sub>2</sub>O and the subducting mantle was modelled as harzburgite + H<sub>2</sub>O. For central Costa Rica, where we have the best tomographic resolution, we then computed  $P$ -wave velocities using a Voigt–Reuss–Hill average (Hill 1952) weighted by mineral proportions and  $P$ – $T$  conditions derived in the previous step (Fig. 14). Velocities obtained following this approach are within 1–2 per cent of rock velocities measured by laboratory experiments (Hacker *et al.* 2003a).

Our predicted  $P$ -wave velocities are lowest within the subducting oceanic crust and the uppermost subducting mantle (Fig. 14) and are associated with mineral parageneses containing the highest H<sub>2</sub>O content (Fig. 13). The location of the predicted low velocities in the subducting slab is a good match for the low velocities observed in our tomographic model along profile C–C', which contains most of the intermediate-depth seismicity (Figs 13 and 14). Consequently, we interpret these low velocities as hydrous rocks of the subducting oceanic crust and upper oceanic mantle. The absolute values of the predicted velocities (6.0–7.3 km s<sup>-1</sup> at 50 km depth) are significantly lower than those computed by tomography (7.0–7.5 km s<sup>-1</sup> at 50 km depth). Predicted velocities are based on the maximum thermodynamically possible H<sub>2</sub>O content, which in reality can certainly yield higher velocities (Hacker *et al.* 2003a).

Our results along profile C–C' are in accord with tomographic images of the Pacific slab under southern Alaska (Kissling & Lahr 1991). The Alaska study also imaged a high-velocity slab underlying a thin low-velocity zone containing most of the WBZ seismicity. Because of the wider aperture of the seismic array in southern Alaska, the high-velocity slab was imaged continuously to greater depth beneath a thin low-velocity layer. Other local earthquake tomography studies do not image a low-velocity zone on top of the high-velocity slab because the vertical depth resolution is more than 10 km (e.g. Protti *et al.* 1996; Graeber & Asch 1999; Schurr 2000) or the top of the subducting slab is *a priori* defined by a high-velocity first-order discontinuity (e.g. Zhao *et al.* 1992, 1995; Nakajima *et al.* 2001). Former studies will image the entire slab as only one pixel, whereas in our study the slab in central Costa Rica consists of two pixels due to closer grid node spacing (10 km) with depth. The

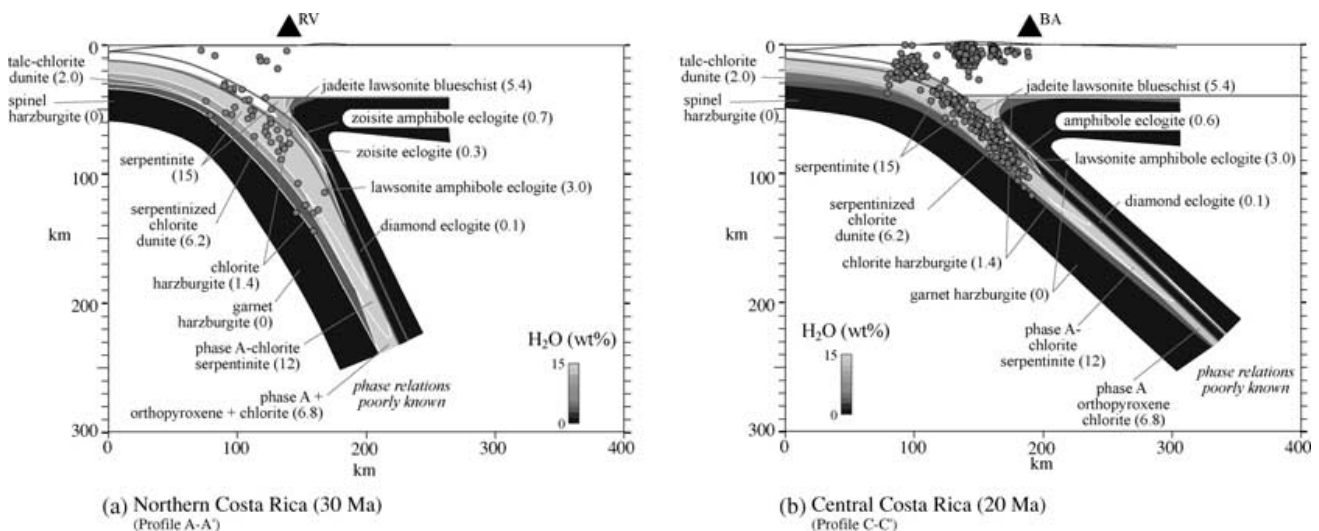


**Figure 13.** Predicted maximum H<sub>2</sub>O content (values for individual minerals are shown in parentheses) for northern and central Costa Rica calculated following Hacker (1996) and Hacker *et al.* (2002a). A slab age of 30 and 20 Ma was assumed for (a) and (b), respectively. Colour coding is proportional to H<sub>2</sub>O content; black shading denotes anhydrous rocks. Seismicity is taken from the profile A–A' (Fig. 11b) and profile C–C' (Fig. 11f) for northern Costa Rica and central Costa Rica, respectively. Black triangles mark Quaternary volcanoes. RV, Rincon de la Vieja; BA, Barba.

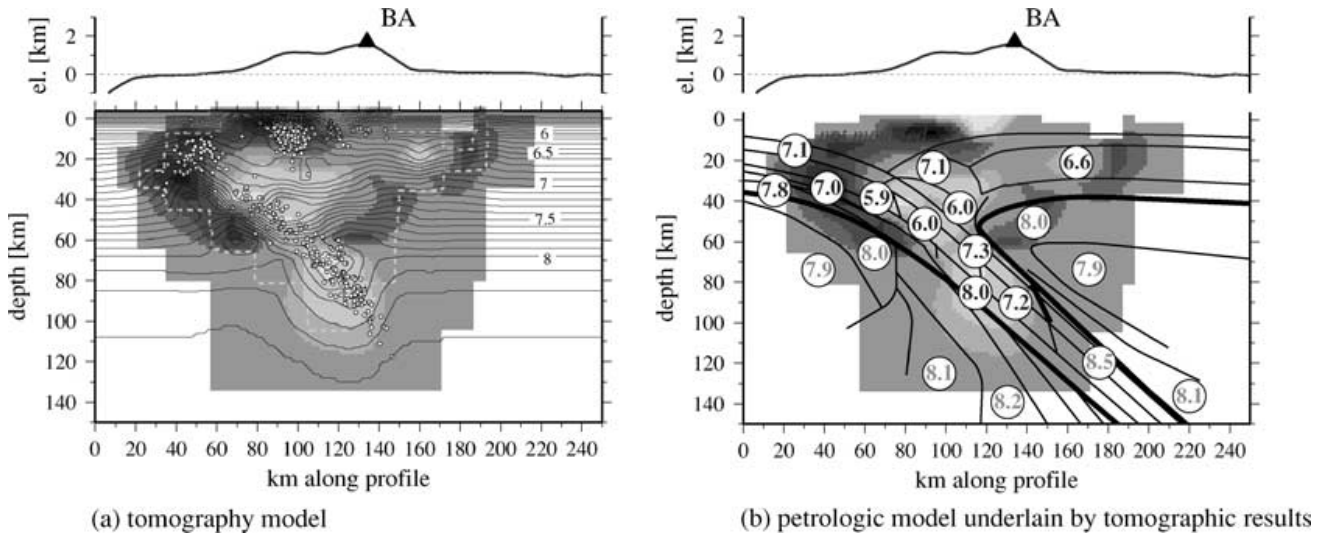


**Figure 14.** (a) Vertical cross-section of the 3-D  $V_p$  model and (b) theoretical  $V_p$  from petrological modelling underlain by tomographic velocity perturbations for central Costa Rica (profile C–C'). Contour lines in (a) denote absolute velocities. Contour interval is  $0.1 \text{ km s}^{-1}$ . Grey and dark numbers in (b) denote velocities of anhydrous and hydrous rocks, respectively. Bold lines mark boundary between hydrous and anhydrous rocks. See the text for a discussion.

existence of a thin low-velocity layer on top of subducting slabs in north Pacific subduction zones is further constrained by the analysis of distorted body waves travelling within the subducting slabs. A thin (1–7 km thick) low-velocity layer, interpreted as hydrated subducting oceanic crust, must remain seismically slow relative to the surrounding mantle to explain the observed signals (Abers 2000).

There is growing evidence that intermediate-depth earthquakes of WBZ are enabled by dehydration (Green & Houston 1995; Kirby *et al.* 1996; Hacker *et al.* 2003b). We plotted the seismicity observed in northern Costa Rica (profile A–A') and central Costa Rica (profile C–C') on top of the predicted equilibrium mineralogy (Fig. 13). For central Costa Rica we find that termination of the WBZ seismicity coincides with the predicted termination of dehydration reactions in the subducting oceanic crust, i.e. complete transformation to eclogite. One might infer from Fig. 13 that intermediate-depth earthquakes occur within the subducting oceanic crust and uppermost oceanic mantle of Costa Rica, but location uncertainties in focal depths as shown below an average of 7 km for central Costa Rica (Fig. 15). These relatively large uncertainties yield a blurred image of the real location of seismicity. We therefore propose that most of the WBZ seismicity in central Costa Rica occurs in the subducting oceanic crust because the maximum seismicity depth corresponds well with the maximum predicted depth for hydrous minerals in the crust. The picture is perhaps less clear in northern Costa Rica, where WBZ seismicity occurs in two clusters, one at 50–70 km depth and one at 140 km depth. Taking into account the larger uncertainties (15 km) in focal depth (Fig. 15), the shallow cluster can be attributed to dehydration reactions in the subducting oceanic crust. Like central Costa Rica, the maximum depth of seismicity corresponds well with the maximum predicted depth for hydrous minerals in the crust; the fact that the lower cluster of seismicity appears to be in the mantle of the downgoing slab may well be an artefact of how the slab shape was guessed from the seismicity (Fig. 11a).

Seismicity in Costa Rica shows a well-defined Wadati–Benioff zone, except for southern Costa Rica, where the station distribution is sparse and the seismicity is low (Figs 11 and 12). Protti *et al.* (1994) postulated the existence of a contortion, the Quesada Sharp

Contortion (QSC), in the subducting Cocos Plate beneath northern Costa Rica (Fig. 12). The Quesada Sharp Contortion separates a deep and steeply dipping slab beneath northern Costa Rica from a shallow and moderately dipping slab beneath central Costa Rica. We find only weak evidence for such a contortion in the subducting Cocos Plate. Envelopes based on the WBZ seismicity could indicate a steeper slab beneath northern Costa Rica below 100 km depth (Fig. 11b), but the seismicity and station distribution in northern Costa Rica is sparse, complicating the use of these contours.

The most obvious feature of the WBZ seismicity is a gradual decrease in maximum depth from northern to southern Costa Rica. Close to the QSC the WBZ seismicity reaches a depth of 120 km, whereas beneath the city of Quepos no WBZ seismicity deeper than 60 km is observed (Figs 12, 11d and j). Further southeast, no clear Wadati–Benioff zone can be detected and seismicity is no deeper than 50 km depth (Figs 12 and 11i). Protti *et al.* (1994) explained the shallowing of the Wadati–Benioff zone beneath central Costa Rica as being the result of differences in age of the subducting Cocos Plate, arguing that the older lithosphere should show a deeper transition from brittle to ductile deformation. As shown above, however, intermediate-depth seismicity within the subducting Cocos Plate may be enabled by dehydration; as a corollary, once the oceanic crust has transformed to anhydrous eclogite dehydration-induced seismicity should stop (Peacock 1990; Hacker *et al.* 2003b). Phase relations dictate that oceanic crust transforms to eclogite at shallower depths in warm subduction zones than in cold subduction zones (Peacock & Wang 1999). Our petrological models (Fig. 13) predict that the oceanic crust transforms to eclogite at a depth of  $\sim 130$  km for northern Costa Rica and at a depth of  $\sim 100$  km for central Costa Rica, even though the subducting plate is only 10 Myr younger beneath central Costa Rica. South of central Costa Rica, however, where the maximum depth of the WBZ seismicity decreases from 120 km depth to 50 km depth, the plate age decreases by only 2 Myr (Barckhausen *et al.* 2001), such that the difference in age of the oceanic lithosphere cannot explain the shallowing of the WBZ seismicity. A possible explanation for this conundrum lies in the tectonic (Johnston & Thorkelson 1997) and geochemical (Abratis & Woerner 2001) evidence that a slab window

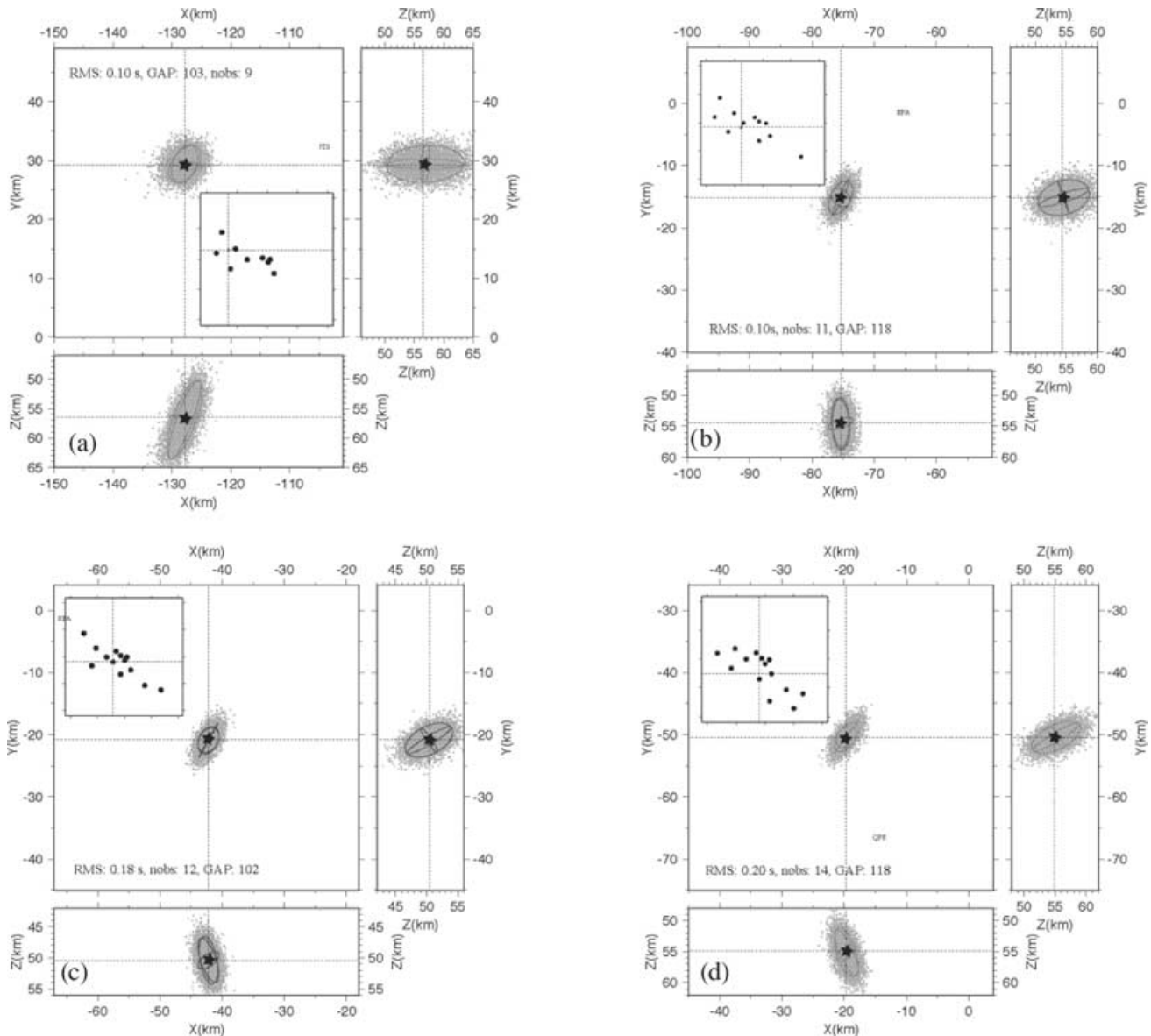


**Figure 15.** Location uncertainties of selected earthquakes of profiles: (a) A–A', (b) B–B', (c) C–C', (d) D–D'. Location uncertainties are presented as density scatter plots (Lomax *et al.* 2000) derived from the *a posteriori* density function. A high density of grey dots denotes a high probability for the hypocentre location. Grey lines show a projection of the 68 per cent confidence ellipsoid. The star marks the maximum-likelihood hypocentre location. Dots in inlay mark the location of stations used to relocate the earthquake. See the text for further discussion of the method.

may have formed beneath southeastern Costa Rica. Pacific asthenosphere from the Galapagos plumehead may be entering through the slab window, explaining not only the presence of ocean-island-type mantle beneath southeastern Costa Rica (Herrstrom *et al.* 1995), but also heating the subducting slab, reducing the depth of eclogite formation, and causing the observed shallowing of the WBZ seismicity. Poor resolution at greater depth in southeastern Costa Rica prevents us from imaging hot asthenospheric material. A similar shallowing of WBZ seismicity is observed in the northwesternmost Pacific, where the Aleutian and Kamchatka arcs meet at an angle of nearly  $90^\circ$  (Yogodzinski *et al.* 2001; Peyton *et al.* 2001). Seismic anisotropy in that area indicates asthenospheric flow around and beneath the disrupted slab edges (Peyton *et al.* 2001), which

may have the same effect on the WBZ seismicity as in central Costa Rica.

### Impact of seafloor morphology on slab structure and WBZ seismicity

Our tomographic images (Figs 10 and 11) reflect the observed complexity of the Cocos Plate, suggesting that the seafloor morphology may have a significant impact not only on the Quaternary tectonics of the continental slope (von Huene *et al.* 2000) but also on the deeper parts of the subduction zone.

Within the smooth segment our results show a smooth picture with large anomalies. The most remarkable feature is a narrow and

shallow low-velocity zone paralleling the subducting Cocos Plate down to a depth of 40 km (Fig. 11a). As can be inferred from Fig. 10, the 30–40 km depth range along the coast is equally well resolved in northern and central Costa Rica. Yet, there is no evidence for a similar zone of low velocities beneath central Costa Rica. We further tested the absence of a shallow low-velocity zone paralleling the subducting slab beneath central Costa Rica by inverting synthetic traveltimes that were derived through a model consisting of a high-velocity slab overlain by a small low-velocity zone beneath the entirety of Costa Rica. The low-velocity zone was well resolved in northern and central Costa Rica. Similar low-velocity zones were interpreted as subducted sediment (Reyners *et al.* 1998). However, seismic refraction work off Nicoya Peninsula (Christeson *et al.* 1999; Sallares *et al.* 2001) indicates only a thin (<0.5 km) sedimentary carapace, consistent with drill cores (Kimura *et al.* 1997). Another plausible explanation is that strong hydration of the oceanic crust may reduce *P*-wave velocities. Heat flow in the frontal part of the subduction zone off the Nicoya Peninsula is anomalously low, suggesting that seawater is circulating within the oceanic crust (Langseth & Silver 1996). Seawater may enter through normal faults seaward of the trench. During subduction the seawater is expelled at shallow depth (<40 km) due to increasing pressure. The fluids may migrate updip along the plate interface, and ultimately be expelled at low-temperature vents on the seafloor off Nicoya Peninsula (Kahn *et al.* 1996). We do not observe a similar low-velocity zone in central or southeastern Costa Rica, suggesting that the oceanic crust is not hydrated or at least not as strongly hydrated as in northwest Costa Rica.

Tomographic images within the seamount-dominated segment of the Cocos Plate show a high complexity (Figs 11c–h). Although the cross-sections are only 50 km apart, each shows a different image. Along profiles B–B' and D–D', small low-velocity anomalies are detected at shallow depth (30 km) close to the subducting slab. A cluster of seismicity is associated with each of the anomalies located directly arcward and separate from the WBZ and crustal seismicity. The low-velocity anomaly along profile B–B' has been identified as a subducted seamount beneath the Gulf of Nicoya, which caused an  $M_w = 7.0$  earthquake in 1990 (Husen *et al.* 2002). Profile D–D' is located in an area struck by an  $M_w = 6.9$  earthquake in 1999 (Fig. 1). Both earthquakes, 1990 and 1999, were nearly equal in magnitude and show similar thrust-type focal mechanisms (Fig. 1), suggesting that the small low-velocity anomaly along profile D–D' may represent a subducted seamount as well. There is no evidence for deep subducted seamounts along profile C–C' (Fig. 11e).

WBZ seismicity along profile C–C' forms a narrow band (Fig. 11f) interpreted to lie within the subducting oceanic crust as discussed earlier. Along profile D–D', however, we observe a much wider band (20 km) of WBZ seismicity, which appears to be clustered in the vicinity of shallow, low *P*-wave velocity anomaly, possibly representing a subducted seamount. An apparent widening of the WBZ seismicity may be observed as well along profile B–B' (Fig. 11d), but this can be a projection artefact caused by the proposed contortion of the subducting slab along the QSC (Fig. 12). The apparent thickening of the seismicity is not an artefact caused by larger location uncertainties along profile D–D'. We relocated seismicity using a non-linear probabilistic approach, which includes a more accurate, non-linear description of location uncertainties (Tarantola & Valette 1982; Lomax *et al.* 2000). The approach computes the *a posteriori* probability density function (PDF) using either a grid search or a global sampling method such as the Metropolis–Gibbs sampler or the Oct–Tree search. Location uncertainties can be presented either as confidence contours or as density scatter plots

(Lomax *et al.* 2000). The latter draws a number of samples from the PDF with the number of samples being proportional to the probability as given by the PDF. Fig. 15 shows similar location uncertainties for three earthquakes located along profiles B–B', C–C' and D–D', indicating that all three earthquakes were located with the same accuracy. The thickness of the WBZ along profile D–D' clearly exceeds the thickness of the subducting oceanic crust even when accounting for the relatively large location uncertainties.

Thickening of the WBZ seismicity along profile D–D' is strongest in the vicinity of the proposed subducted seamount, which suggests a possible link between subducting of a seamount and the thickening of WBZ seismicity. Seamounts represent highly altered and fractured oceanic crust. Once subducted, the excess mass and buoyancy of a seamount will increase the normal stress, leading to the rupture of large subduction earthquakes (Cloos 1992; Husen *et al.* 2002). Increased normal stress may also reactivate fractures associated with the formation of a seamount, producing many small earthquakes in the vicinity of subducted seamounts. A detailed analysis of focal mechanisms would be needed to further constrain this hypothesis, but this would be beyond the scope of this paper.

### Source regions for active volcanism in Costa Rica

The current understanding of arc magmatism is that fluids released by slab dehydration migrate into the overlying mantle wedge, lower the solidus of the peridotite and trigger partial melting (Gill 1981). It is still debated how a partial melt finally ascends through the mantle wedge and reaches the surface. Aqueous fluids and silicate liquids significantly alter the elastic and anelastic properties of rocks, changing the seismic velocities. In recent tomographic studies, low *P*- and *S*-wave velocities have been interpreted as indicating the existence of partial melts in the mantle wedge and overlying crust beneath active volcanoes (Iwamori & Zhao 2000; Schurr 2000; Nakajima *et al.* 2001). In central Costa Rica, we observe large, low *P*-wave velocity anomalies in the uppermost mantle and overlying crust beneath the southeastern volcanoes Poas, Barba, Irazu and Turrialba (Figs 10, 11e and g). Absolute velocities are as low as  $6.5 \text{ km s}^{-1}$  at 30 km depth beneath the volcanic arc. Beneath Arenal volcano, low *P*-wave velocities are restricted to the crust (Fig. 11c). In northwestern Costa Rica, the resolution in the mantle wedge and overlying crust is too poor to adequately resolve low *P*-wave velocities associated with partial melt (Fig. 11a). Our petrological model for central Costa Rica predicts hydrated, serpentine- and/or chlorite-bearing mantle in a narrow zone just above the subducting slab and in a larger area in the 'tip' of the mantle wedge; the rest of the mantle wedge should have few hydrous minerals (Fig. 13). Our tomographic model for this same cross-section shows excellent correspondence between the areas of predicted hydrous minerals and low velocities and areas of predicted anhydrous minerals and high velocities in the mantle wedge (Fig. 14). The absolute velocities observed in the tomography model are faster than predicted in the petrological model, surely reflecting less hydration than the assumed maximum  $\text{H}_2\text{O}$  content used in the petrological model. In general, the agreement between the observed velocities and the predicted velocities indicates that the tomography is, to first order, imaging the locations of hydrous minerals, or, potentially, hydrous fluids associated with the decomposition of hydrous minerals within the mantle wedge beneath central Costa Rica.

The above interpretation only uses tomographic images of central Costa Rica. However, tomographic images along profile B–B' to the north show that the mantle wedge may not be hydrated everywhere. Low velocities ( $\sim 7 \text{ km s}^{-1}$  at 40 km depth) within the mantle wedge

along profile C–C' are replaced by high velocities ( $\sim 7.5 \text{ km s}^{-1}$  at 40 km depth) along profile B–B' (Figs 10 and 11). The possible existence of an anhydrous mantle wedge along profile B–B' is supported by the small volume of Arenal volcano (Carr & Stoiber 1990) and a small gap between active volcanoes to the northeast and to the southeast (Fig. 2).

Within a small area, lavas from Nicaragua and Costa Rica show a dramatic variation in their geochemistry (Carr & Stoiber 1990; Herrstrom *et al.* 1995; Patino *et al.* 2000) with a mantle composition beneath Nicaragua inferred to be similar to mid-ocean-ridge basalt (MORB) and similar to ocean island basalt (OIB) beneath central Costa Rica. In between, lavas show irregular compositions forming a transition zone between Nicaragua and central Costa Rica. The different mantle compositions beneath Nicaragua and Costa Rica may result from infiltration of the Pacific asthenosphere beneath central Costa Rica (Herrstrom *et al.* 1995) or by melting at shallow depth (Leeman & Carr 1995). Our results confirm that melt generation beneath central Costa Rica is likely to be shallow because of the presence of a shallow hydrated mantle wedge. The characteristics of the transition zone between Costa Rica and Nicaragua can be explained by the ongoing subduction of Fisher Ridge and the related absence of a hydrated mantle wedge beneath the transition zone. Magmas from both regions possibly mix at the base of the lower crust beneath the transition zone as indicated by the low velocities found beneath Arenal volcano.

## CONCLUSIONS

Tomographic results presented in this study show a complex lithospheric structure beneath Costa Rica. To first order, the complexity can be explained by differences in the structure and evolution of the incoming Cocos Plate. Physical segmentation of the incoming Cocos Plate (von Huene *et al.* 2000) into a smooth segment, a seamount-dominated segment and a Cocos ridge influenced segment is clearly reflected in the tomographic results. Northwestern Costa Rica shows a smooth lithospheric structure with a steep and deeply penetrating slab. The high density of seamounts off central Costa Rica and their subsequent subduction are responsible for a complex lithospheric structure beneath central Costa Rica. The common picture of a narrow Wadati–Benioff zone located in the subducting oceanic crust and a possibly hydrated oceanic crust at intermediate depth is distorted by the presence of subducted seamounts. Relatively low velocities represent the subducting Cocos Plate in southeastern Costa Rica as opposed to high velocities in central and northwestern Costa Rica. These low velocities are caused by the unusually thick oceanic crust and relatively young crustal ages of the subducting Cocos ridge.

In central and northwestern Costa Rica there is a good correlation between the locations of intermediate-depth earthquakes and the predicted locations of hydrous minerals. This suggests that intermediate-depth seismicity in central and northwestern Costa Rica is enabled by dehydration. Most of the intermediate-depth seismicity beneath central Costa Rica lies within a low-velocity zone. We interpreted this zone of low velocities as evidence for a hydrous upper oceanic crust. There are only a few studies (Kissling & Lahr 1991; Abers 2000) showing seismological evidence of a hydrous upper oceanic crust either due to limitations in the resolution (e.g. Protti *et al.* 1996; Graeber & Asch 1999; Schurr 2000) or due to defining the top of the subducting slab as a high-velocity first-order discontinuity (e.g. Zhao *et al.* 1992, 1995; Nakajima *et al.* 2001).

The southeastward shallowing of WBZ seismicity from 120 km depth to 50 km depth cannot be explained by the insignificant 2 Myr age difference of the subducting Cocos Plate (Protti *et al.* 1995). It is more likely to be related to asthenospheric flow through a proposed slab window beneath southeastern Costa Rica that heats the plate and causes increasingly shallow depths of dehydration.

Our tomographic and petrological models may constrain the formation of partial melt beneath central Costa Rica to shallow depth (60 km) as indicated by the evidence of a small and shallow, hydrated mantle wedge. Ongoing subduction of the Fisher Ridge and associated seamounts—the rough–smooth boundary—results in an anhydrous mantle wedge beneath Arenal volcano separating different mantle domains beneath central Costa Rica and northwestern Costa Rica and Nicaragua. Further studies of more parameters, however, such as the *P*- to *S*-wave velocity ratio and attenuation are needed to more reliably resolve the differences in the physical state of the mantle wedge beneath Costa Rica. Work at other subduction zones (Iwamori & Zhao 2000; Schurr 2000; Haberland & Rietbrock 2001; Nakajima *et al.* 2001) have successfully demonstrated that *P*- to *S*-wave velocity ratios and attenuation are much more sensitive to temperature and the presence of fluids, thus allowing a much more reliable assessment of the physical parameters within the mantle wedge.

## ACKNOWLEDGMENTS

We thank the staff of OVSICORI-UNA, RSN, INETER, UPA and CASC centre for providing seismic data and network information. We thank Steven Ward and two anonymous reviewers for their thoughtful and excellent comments, which significantly improved the manuscript. We thank S. Peacock for making his thermal models available. Figures were generated using the GMT software by Wessel & Smith (1998). The work was supported by ETH Zurich, Switzerland.

## REFERENCES

- Abers, G.A., 2000. Hydrated subducted crust at 100–250 km depth, *Earth planet. Sci. Lett.*, **176**, 323–330.
- Abers, G.A. & Roecker, S.W., 1991. Deep structure of an arc-continent collision: earthquake relocation and inversion for upper mantle *P* and *S* wave velocities beneath Papua New Guinea, *J. geophys. Res.*, **96**, 6379–6401.
- Abratis, M. & Woerner, G., 2001. Ridge collision, slab-window formation, and the flux of Pacific asthenosphere into the Caribbean realm, *Geology*, **29**, 127–130.
- Barckhausen, U., Roeser, H.A. & von Huene, R., 1998. Magnetic signature of upper plate structures and subducting seamounts at the convergent margin off Costa Rica, *J. geophys. Res.*, **103**, 7079–7094.
- Barckhausen, U., Ranero, C., von Huene, R., Cande, S.C. & Roeser, H.A., 2001. Revised tectonic boundaries in the Cocos Plate off Costa Rica: implications for the segmentation of the convergent margin and for plate tectonic models, *J. geophys. Res.*, **106**, 19 207–19 220.
- Bijwaard, H., Spakman, W. & Engdahl, R.E., 1998. Closing the gap between regional and global traveltimes tomography, *J. geophys. Res.*, **103**, 30 055–30 078.
- Carr, M.J. & Stoiber, R.E., 1990. Volcanism, in *The Caribbean Region*, eds Dengo, G. & Case, J.E., Geological Society of America, Boulder.
- Christeson, G.L., McIntosh, K.D., Flueh, E.R. & Godde, H., 1999. Structure of the Costa Rica convergent margin, offshore Nicoya Peninsula, *J. geophys. Res.*, **104**, 25 443–25 468.
- Cloos, M., 1992. Thrust-type subduction-zone earthquakes and seamount asperities: a physical model for seismic rupture, *Geology*, **20**, 601–604.

- Colombo, D., Cimini, G.B. & de Franco, R., 1997. Three-dimensional velocity structure of the upper mantle beneath Costa Rica from a teleseismic tomography study, *Geophys. J. Int.*, **131**, 189–208.
- Davies, J.H., 1999. The role of hydraulic fractures and intermediate-depth earthquakes in generating subduction-zone magmatism, *Nature*, **398**, 142–144.
- De Mets, C., 2001. A new estimate for present-day Cocos–Caribbean Plate motion: implications for slip along the central American volcanic arc, *Geophys. Res. Lett.*, **28**, 4043–4046.
- Duncan, R.A. & Hargraves, R.B., 1984. Plate tectonic evolution of the Caribbean region in the mantle reference frame, *Mem. Geol. Soc. Am.*, **162**, 81–93.
- Eberhart-Phillips, D., 1986. Three-dimensional velocity structure in northern California Coast Range from inversion of local earthquake arrival times, *Bull. seism. Soc. Am.*, **76**, 1025–1052.
- Eberhart-Phillips, D., 1990. Three-dimensional *P* and *S* velocity structure in the Coalinga Region, California, *J. geophys. Res.*, **95**, 15 343–15 363.
- Fan, G., Beck, S. & Wallace, T.C., 1993. The seismic source parameters of the 1991 Costa Rica aftershock sequence: evidence for a transcurrent plate boundary, *J. geophys. Res.*, **98**, 15 759–15 778.
- Gill, J.B., 1981. *Orogenic Andesites and Plate Tectonics*, Springer-Verlag, Berlin.
- Goes, S.D.B., Velasco, A., Schwartz, S.Y. & Lay, T., 1993. The April 22, 1991, Valle de la Estrella, Costa Rica ( $M_w = 7.7$ ) earthquake and its tectonic implications: a broadband seismic study, *J. geophys. Res.*, **98**, 8127–8142.
- Graeber, F. & Asch, G., 1999. Three-dimensional models of *P*-wave velocity and *P*-to-*S* velocity ratio in the southern central Andes by simultaneous inversion of local earthquake data, *J. geophys. Res.*, **104**, 20 237–20 256.
- Green, H. & Houston, H., 1995. The mechanics of deep earthquakes, *Ann. Rev. Earth Sci.*, **23**, 169–213.
- Haberland, C. & Rietbrock, A., 2001. Attenuation tomography in the western central Andes: a detailed insight into the structure of a magmatic arc, *J. geophys. Res.*, **106**, 11 151–11 167.
- Hacker, B.R., 1996. Eclogite formation and the rheology, buoyancy, seismicity, and  $H_2O$  content of oceanic crust, in *Subduction Top to Bottom*, pp. 337–346, eds Bebout, G., Scholl, D., Kirby, S. & Platt, J., American Geophysical Union.
- Hacker, B.R., Peacock, S.M. & Abers, G.A., 2003a. Subduction factory 1. Theoretical mineralogy, density, seismic wave speeds, and  $H_2O$  content, *J. geophys. Res.*, **108**, doi: 10.1029/2001JB001127.
- Hacker, B.R., Peacock, S.M. & Abers, G.A., 2003b. Subduction factory 2. Intermediate-depth earthquakes in subducting slabs are linked to metamorphic dehydration reactions, *J. geophys. Res.*, **108**, doi: 10.1029/2001JB001129.
- Haslinger, F. & Kissling, E., 2001. Investigating effects of 3-D ray tracing methods in local earthquake tomography, *Phys. Earth planet. Inter.*, **123**, 103–114.
- Haslinger, F. *et al.*, 1999. 3-D crustal structure from local earthquake tomography around Gulf of Arta (Ionian region, NW Greece), *Tectonophysics*, **304**, 210–218.
- Herrstrom, E.A., Reagan, M.K. & Morris, J.D., 1995. Variations in lava composition associated with flow of asthenosphere beneath southern Central America, *Geology*, **23**, 617–620.
- Hey, R., 1977. Tectonic evolution of the Cocos-Nazca spreading center, *Geol. Soc. Am. Bull.*, **88**, 1404–1420.
- Hill, R., 1952. The elastic behavior of crystalline aggregates, *Phil. Trans. R. Soc. Lond., A.*, **65**, 349–354.
- Humphreys, E. & Clayton, R.W., 1988. Adaptation of back projection tomography to seismic travel time problems, *J. geophys. Res.*, **93**, 1073–1085.
- Husen, S., Kissling, E., Flueh, E.R. & Asch, G., 1999. Accurate hypocentre determination in the seismogenic zone of the subducting Nazca Plate in northern Chile using a combined on-/offshore network, *Geophys. J. Int.*, **138**, 687–701.
- Husen, S., Kissling, E. & Flueh, E.R., 2000. Local earthquake tomography of shallow subduction in north Chile: a combined onshore and offshore study, *J. geophys. Res.*, **105**, 28 183–28 198.
- Husen, S., Quintero, R. & Kissling, E., 2002. Tomographic evidence for a subducted seamount beneath the Gulf of Nicoya, Costa Rica: the cause of the 1990  $M_w = 7.0$  Gulf of Nicoya earthquake, *Geophys. Res. Lett.*, **29**, doi: 10.1029/2001GL014 045.
- Iwamori, H. & Zhao, D., 2000. Melting and seismic structure beneath the northeast Japan arc, *Geophys. Res. Lett.*, **27**, 425–428.
- Johnston, S.T. & Thorkelson, D.J., 1997. Cocos-Nazca slab window beneath Central America, *Earth planet. Sci. Lett.*, **146**, 465–474.
- Kahn, L.M., Silver, E.A., Orange, D., Kochevar, R. & McAdoo, B., 1996. Surficial evidence of fluid expulsion from the Costa Rica accretionary prism, *Geophys. Res. Lett.*, **23**, 887–890.
- Kimura, G. *et al.*, 1997. *Proc. Ocean Drilling Program, Initial Reports* 170, Ocean Drill. Program, College Station.
- Kirby, S., Engdahl, R.E. & Denlinger, R., 1996. Intermediate-depth intraslab earthquakes and arc volcanism as physical expression of crustal and uppermost mantle metamorphism in subducting slabs, in *Subduction: Top to Bottom*, pp. 195–214, eds Bebout, G., Scholl, D., Kirby, S. & Platt, J., American Geophysical Union.
- Kissling, E., 1988. Geotomography with local earthquake data, *Rev. Geophys.*, **26**, 659–698.
- Kissling, E. & Lahr, J.C., 1991. Tomographic image of the Pacific slab under southern Alaska, *Eclogae Geol. Helv.*, **84**, 297–315.
- Kissling, E., Husen, S. & Haslinger, F., 2001. Model parameterization in seismic tomography: a choice of consequences for the solution quality, *Phys. Earth planet. Inter.*, **123**, 89–101.
- Kissling, E., Ellsworth, W.L., Eberhart-Phillips, D. & Kradolfer, U., 1994. Initial reference models in local earthquake tomography, *J. geophys. Res.*, **99**, 19 635–19 646.
- Kolarsky, R.A., Mann, P. & Montero, W., 1995. Island arc response to shallow subduction of the Cocos Ridge, Costa Rica, in *Geologic and Tectonic Development of the Caribbean Plate Boundary in Southern Central America*, pp. 235–261, ed. Mann, P., Geological Society of America, Boulder.
- Langseth, M.G. & Silver, E.A., 1996. The Nicoya convergent margin—a region of exceptionally low heat flow, *Geophys. Res. Lett.*, **23**, 891–894.
- Leeman, W.P. & Carr, M.J., 1995. Geochemical constraints on subduction processes in the Central American volcanic arc: implications of boron geochemistry, in *Geologic and Tectonic Development of the Caribbean Plate Boundary in Southern Central America*, pp. 57–73, ed. Mann, P., Geological Society of America, Boulder.
- Leveque, J.-J., Rivera, L. & Wittlinger, G., 1993. On the use of the checkerboard test to assess the resolution of tomographic inversions, *Geophys. J. Int.*, **115**, 313–318.
- Lomax, A., Virieux, J., Volant, P. & Thierry-Berge, C., 2000. Probabilistic earthquake location in 3-D and layered models, in *Advances in Seismic Event Location*, pp. 101–134, eds Thurber, C.H. & Rabinowitz, N., Kluwer, Dordrecht.
- Marshall, J.S., Fisher, D.M. & Gardner, T.W., 2000. Central Costa Rica deformed belt: kinematics of diffuse faulting across the western Panama block, *Tectonics*, **19**, 468–492.
- Michellini, A. & McEvilly, T.V., 1991. Seismological studies at Parkfield. I. Simultaneous inversion for velocity structure and hypocenters using cubic B-splines parameterization, *Bull. seism. Soc. Am.*, **81**, 524–552.
- Nakajima, J., Matsuzawa, T., Hasegawa, A. & Zhao, D., 2001. Three-dimensional structure of  $V_p$ ,  $V_s$ , and  $V_p/V_s$  beneath northeastern Japan: implications for arc magmatism and fluids, *J. geophys. Res.*, **106**, 21 843–21 857.
- Patino, L.C., Carr, M.J. & Feigenson, M.D., 2000. Local and regional variations in Central American arc lavas controlled by variations in subducted sediment input, *Contrib. Mineral. Petrol.*, **138**, 265–283.
- Peacock, S.M., 1990. Fluid processes in subduction zones, *Science*, **248**, 329–337.
- Peacock, S.M., 1996. Thermal and petrologic structure of subduction zones, in *Subduction: Top to Bottom*, pp. 119–133, eds Bebout, G., Scholl, D., Kirby, S. & Platt, J., American Geophysical Union, Washington, DC.
- Peacock, S.M. & Wang, K., 1999. Seismic consequences of warm versus cool subduction metamorphism: examples from southwest and northeast Japan, *Science*, **286**, 937–939.

- Peyton, V., Levin, V., Park, J., Brandon, M., Lees, J.M., Gordeev, E. & Ozerov, A., 2001. Mantle flow at slab edge: seismic anisotropy in the Kamchatka region, *Geophys. Res. Lett.*, **28**, 379–382.
- Podvin, P. & Lecomte, I., 1991. Finite difference computation of travel times in very contrasted velocity models: a massively parallel approach and its associated tools, *Geophys. J. Int.*, **105**, 271–284.
- Protti, M., Güendel, F. & McNally, K., 1994. The geometry of the Wadati–Benioff zone under southern Central America and its tectonic significance: results from a high-resolution local seismographic network, *Phys. Earth planet. Inter.*, **84**, 271–287.
- Protti, M., Guendel, F. & McNally, K., 1995. Correlation between the age of the subducting Cocos Plate and the geometry of the Wadati–Benioff zone under Nicaragua and Costa Rica, in *Geologic and Tectonic Development of the Caribbean Plate Boundary in Southern Central America*, pp. 309–326, ed. Mann, P., Geological Society of America, Boulder.
- Protti, M., Schwartz, S.Y. & Zandt, G., 1996. Simultaneous inversion for earthquake location and velocity structure beneath central Costa Rica, *Bull. seism. Soc. Am.*, **86**, 19–31.
- Quintero, R. & Kissling, E., 2001. An improved *P*-wave velocity reference model for Costa Rica, *Geofísica Int.*, **40**, 3–19.
- Ranero, C.R. & von Huene, R., 2000. Subduction erosion along the Middle America convergent margin, *Nature*, **404**, 748–752.
- Reyners, M., Eberhart-Phillips, D. & Stuart, G., 1998. A three-dimensional image of the shallow subduction: crustal structure of the Raukumara Peninsula, New Zealand, *Geophys. J. Int.*, **137**, 873–890.
- Sallares, V., Danobeitia, J.J. & Flueh, E.R., 2001. Lithospheric structure of the Costa Rican Isthmus: effects of subduction zone magmatism on an oceanic plateau, *J. geophys. Res.*, **106**, 621–643.
- Schurr, B., 2000. Seismic structure of the central Andean subduction zone from local earthquake data, *Scientific Technical Report*, STR01/01, Geoforschungszentrum, Potsdam.
- Stavenhagen, A.U., Flueh, E.R., Ranero, C., McIntosh, K.D., Shipley, T., Leandro, G., Schulze, A. & Danobeitia, J.J., 1998. Seismic wide-angle investigations in Costa Rica—a crustal velocity model from the Pacific to the Caribbean coast, *Zbl. Geol. Paläont.*, **1**, 393–408.
- Tarantola, A. & Valette, B., 1982. Inverse problems = quest for information, *J. Geophys.*, **50**, 159–170.
- Thurber, C.H., 1983. Earthquake locations and three-dimensional crustal structure in the Coyote Lake area, central California, *J. geophys. Res.*, **88**, 8226–8236.
- Thurber, C.H., 1992. Hypocenter-velocity structure coupling in local earthquake tomography, *Phys. Earth planet. Inter.*, **75**, 55–62.
- Toomey, D.R. & Foulger, G.R., 1989. Tomographic inversion of local earthquake data from the Hengill-Grensadalur Central Volcano Complex, Iceland, *J. geophys. Res.*, **94**, 17 497–17 510.
- Virieux, J. & Farra, V., 1991. Ray tracing in 3-D complex isotropic media: an analysis of the problem, *Geophysics*, **56**, 2057–2069.
- von Huene, R. *et al.*, 1995. Morphotectonic features of the Costa Rican Pacific margin surveyed during Sonne 76 cruise, in *Geologic and Tectonic Development of the Caribbean Plate Boundary in Southern Central America*, pp. 291–308, ed. Mann, P., Geological Society of America, Boulder.
- von Huene, R., Ranero, C.R. & Weinrebe, W., 2000. Quaternary convergent margin tectonics of Costa Rica, segmentation of the Cocos Plate, and Central American volcanism, *Tectonics*, **19**, 314–334.
- Walther, C.H., Bialas, J. & Flueh, E.R., 2000. Crustal structure of the Cocos Ridge off Costa Rica—preliminary results from a seismic wide-angle experiment, *EOS, Trans. Am. geophys. Un.*, Fall Meet. Suppl., **81**, Abstract T11A-03.
- Wessel, P. & Smith, W.H.F., 1998. New improved version of the Generic Mapping Tools released, *EOS Trans. Am. geophys. Un.*, **79**, 579.
- Weyl, R., 1980. *Geology of Central America*, 371, Gebrueder Borntraeger, Berlin.
- Yao, Z.S., Quintero, R. & Roberts, R.G., 1999. Tomographic imaging of *P*- and *S*-wave velocity structure beneath Costa Rica, *J. Geodyn.*, **3**, 177–190.
- Yogodzinski, G.M., Lees, J.M., Churikova, T.G., Dorendorf, F., Woerner, G. & Volynets, O.N., 2001. Geochemical evidence for the melting of subducting oceanic lithosphere at plate edges, *Nature*, **409**, 500–504.
- Zelt, C.A., 1998. Lateral velocity resolution from three-dimensional seismic refraction data, *Geophys. J. Int.*, **135**, 1101–1112.
- Zhao, D., Hasegawa, A. & Horiuchi, S., 1992. Tomographic imaging of *P* and *S* wave velocity structure beneath northeastern Japan, *J. geophys. Res.*, **97**, 19 909–19 928.
- Zhao, D., Christensen, D. & Pulpan, H., 1995. Tomographic imaging of the Alaska subduction zone, *J. geophys. Res.*, **100**, 6487–6504.
- Zhao, D., Asamori, K. & Iwamori, H., 2000. Seismic structure and magmatism of the young Kyushu subduction zone, *Geophys. Res. Lett.*, **27**, 2057–2060.